Self-ubiquitination of a pathogen type-III effector traps and blocks the autophagy machinery to promote disease

Jia Xuan Leong[1], Margot Raffeiner[2], Daniela Spinti[2], Gautier Langin[1], Mirita Franz-Wachtel[3], Andrew R. Guzman[4], Jung-Gun Kim[4], Pooja Pandey[5], Alyona E. Minina[6], Boris Macek[3], Anders Hafrén[8], Tolga O. Bozkurt[5], Mary Beth Mudgett[4], Frederik Börnke[2,7], Daniel Hofius[8], Suayib Üstün[1*]

[1]University of Tübingen, Center for Plant Molecular Biology (ZMBP), 72076 Tübingen, Germany
[2]Leibniz-Institute of Vegetable and Ornamental Crops (IGZ), 14979 Großbeeren, Germany
[3]Interfaculty Institute for Cell Biology, Department of Quantitative Proteomics, University of Tübingen, 72076 Tübingen, Germany.
[4]Department of Biology, Stanford University, Stanford, CA 94305, USA
[5]Department of Life Sciences, Imperial College London, SW7 2AZ London, United Kingdom.
[6]Department of Molecular Sciences, Uppsala BioCenter, Swedish University of Agricultural Sciences and Linnean Center for Plant Biology, 75007 Uppsala, Sweden.
[7]Institute of Biochemistry and Biology, University of Potsdam, 14476 Potsdam, Germany
[8]Department of Plant Biology, Uppsala BioCenter, Swedish University of Agricultural Sciences and Linnean Center for Plant Biology, 75007 Uppsala, Sweden.

Keywords: Autophagy, Effectors, Immunity, Ubiquitination, Disease, Xenophagy

*corresponding author
suayib.uestuen@zmbp.uni-tuebingen.de

Abstract:
Beyond its role in cellular homeostasis, autophagy is considered to play anti- and pro-microbial roles in host-microbe interactions, both in animals and plants. One of the prominent roles of anti-microbial autophagy in animals is to degrade intracellular pathogens or microbial molecules, in a process termed "xenophagy". Consequently, microbes evolved mechanisms to hijack or modulate autophagy to escape elimination. However, the extent to which xenophagy contributes to plant-bacteria interactions remains unknown. Here, we provide evidence that NBR1/Joka2-dependent selective autophagy functions in plant defence by degrading the bacterial type-III effector (T3E) XopL from *Xanthomonas campestris* pv. *vesicatoria (Xcv)*. We show how XopL associates with the autophagy machinery and undergoes self-ubiquitination, subsequently triggering its own degradation by NBR1/Joka2-mediated selective autophagy. Intriguingly, *Xcv* is also able to suppress autophagy in a T3E-dependent manner by utilizing the same T3E XopL that interacts and degrades the autophagy component SH3P2 via its E3 ligase activity. Thus, XopL is able to escape its own degradation and promote pathogenicity of *Xcv* by inhibiting autophagy through SH3P2 depletion. Together, we reveal a novel phenomenon how NBR1/Joka2 contributes to anti-bacterial autophagy and provide a unique mechanism how a T3E undergoes self-modification to act as a bait to trap host cellular degradation machineries.

Significant statement

Autophagy has anti- and pro-microbial roles in host-microbe interactions. Its anti-microbial role is derived from its ability to degrade intracellular pathogens, termed “xenophagy”. The contribution of xenophagy to host-bacteria interactions in plants and its substrates remains elusive. Here, we reveal that NEIGHBOR OF BRCA1 (NBR1)-mediated autophagy has an anti-microbial role towards bacteria by degrading the type-III effector (T3E) XopL from *Xanthomonas campestris* pv. *vesicatoria (Xcv).* We unveil that the same T3E is able to perturb autophagy to escape its own degradation and to boost bacterial virulence. These findings highlight a novel role of xenophagy that is conserved across kingdoms and we offer new perspectives on how T3Es undergo self-modification to trap host cellular degradation pathways.

Introduction

Eukaryotic cells react dynamically to external and internal stimuli by adjusting their proteome. This requires a stringent regulation of protein homeostasis which is achieved by regulated protein degradation. Cellular degradation machineries including the proteasome and autophagy maintain protein homeostasis by recycling unwanted or dysfunctional proteins (1). While the proteasome degrades short-lived proteins or mis-folded proteins, autophagy can remove larger protein complexes, insoluble aggregates, entire organelles as well as pathogens. Under normal conditions, both degradation pathways are critical for cellular housekeeping functions, while under stress conditions they facilitate the reorganization of the proteome to adapt to a changing environment (2).

Regulated proteolytic degradation by proteasome has been identified as an essential component of immunity influencing the outcome of host-microbe interactions in across kingdoms (3, 4). In the recent years, autophagy has also emerged as a central player in immunity and disease in humans and plants (5-9). In mammals, autophagy has various connections to a number of diseases, regulating cell death and innate immunity (7, 10). Dual roles have also been ascribed to autophagy in host-bacteria interactions (11). While some bacterial pathogens recruit the autophagy machinery in order to create a replicative niche (pro-bacterial autophagy), anti-bacterial autophagy removes bacterial intruders to limit pathogen infection (12). The elimination of bacteria is a selective autophagy response, termed xenophagy (13). In this process, bacterial pathogens such as *Salmonella* and *Shigella* are degraded by autophagy through a ubiquitin-dependent mechanism (14, 15). This demonstrates that autophagy is not only a largely unspecific ("bulk") catabolic and recycling process, as increasing evidence now indicates that autophagy also acts as a selective mechanism to degrade protein aggregates, organelles and pathogens. Selectivity is mediated by autophagy receptors, of which p62 and NBR1 play key roles in controlling pathogenic infection in mammals (13). Both autophagy receptors can bind to ubiquitinated bacteria, and degrade them, through their ability to bind autophagosome-associated ATG8 proteins (13).

Plants possess a homologue of NBR1 that was recently described to be involved in plant immunity. Plant NBR1, which is also referred as Joka2 in solanaceous species, is able to restrict growth and disease progression of the plant pathogenic oomycete *Phytophthora infestans*, the bacterium *Pseudomonas syringae* pv. *tomato (Pst)*, and plant viruses such as turnip mosaic virus (TuMV) and cauliflower mosaic virus (CaMV) (16-20). These studies demonstrated that, similar to that in mammals, plant NBR1 participates in xenophagy by degrading viral proteins. Whether NBR1-mediated xenophagy also plays a role in plant-bacteria interactions remains to be determined. This is complicated by the fact that bacteria reside in the extracellular spaces of plant tissues and might not be directly targeted by xenophagy.

It is known that type-III effector (T3E) proteins of plant pathogenic bacteria are present in the host cell. These effectors are able to manipulate host defense responses for the benefit of the pathogen (21). Very recently, it has been shown that microbial effectors perturb or hijack degradation machineries to attenuate plant immune reactions (22, 23). For instance, *Pst* activates autophagy via the action of the T3E HopM1 to degrade the proteasome and suppress its function in a process termed proteaphagy (18, 24). Although this process can be categorized as a pro-bacterial role of autophagy, NBR1-mediated anti-bacterial autophagy seems to restrict lesion formation and pathogenicity of *Pst* (25). The dual role of autophagy in plant-bacteria interactions is further confirmed by findings that certain effectors are also able to suppress autophagy responses, although the understanding of the exact molecular mechanisms are still very limited (26).

Like *Pst*, *Xanthomonas campestris* pv. *vesicatoria (Xcv)* is another well-studied hemi-biotrophic bacterium, causing disease on tomato and pepper plants (27). Mounting evidence has been established that *Xcv* and its T3Es exploit plant ubiquitin- and ubiquitin-like pathways (28, 29). While the role of the proteasome system in *Xanthomonas* infections is well understood,

little is known about how autophagy shapes the outcome of *Xanthomonas*-host interactions. Recent findings in the cassava- *Xanthomonas axonopodis* pv. *manihotis* (*Xam*) model suggest that autophagy has an anti-bacterial role *(30, 31)*. However, our current understanding about how T3Es might modulate and regulate this response is very limited. Are there similar mechanisms operating in pro- and antibacterial roles across different pathogenic bacteria? Do plants utilize xenophagy as an anti-bacterial mechanism to degrade pathogenic components in plant-bacteria interactions?

To address these questions, we performed a mechanistic analysis of the interplay of plant autophagy and *Xcv* pathogenesis. Here, we provide evidence that NBR1/Joka2 degrades T3E XopL, which undergoes self-ubiquitination *in planta*. However, *Xcv* utilizes the same T3E XopL to dampen autophagy by degrading autophagy component SH3P2 in a proteasome-dependent manner via its E3 ligase activity. This rescues T3E XopL from being targeted for degradation by the selective autophagy receptor NBR1/Joka2 and enhances the virulence of *Xcv* in plants. We provide a novel example of how a bacterial T3E traps the autophagy pathway by self-ubiquitination and targeting itself to the NBR1-mediated selective autophagy pathway.

Results

Xanthomonas blocks autophagy in an effector-dependent manner to promote pathogenicity

Given the prominent role of autophagy in host-microbe interactions, we investigated different autophagy responses after Xanthomonas infection. To this end we used the model plant *Nicotiana benthamiana*, as Agrobacterium-mediated transient expression, Virus-induced gene silencing (VIGS), autophagy assays and the use of antibodies are well established and reproducible. Assays were conducted with a *Xcv* strain harboring a deletion in the T3E XopQ (*Xcv ΔxopQ)*, which is a host range determinant in *Nicotiana* species (32). In the absence of XopQ, *Xcv* is fully virulent in *Nicotiana benthamiana* leaves. First, we utilized a quantitative autophagy assay to measure autophagic turnover during infection. This assay is based on Agrobacterium-mediated transient expression of *Renilla* luciferase (RLUC) fused to ATG8a (RLUC-ATG8a) or NBR1 (RLUC-NBR1) together with free *Firefly* luciferase (FLUC) in *N. benthamiana* leaves, which serves as an internal control (18, 33). We also used the previously described autophagy suppressor AIMp, derived from the *Phytophthora* PexRD54 effector (34), as a control for autophagy suppression. Simultaneous measurements in the dual-luciferase system revealed that *Xcv ΔxopQ* infection in leaves expressing the autophagy reporters led to a significant increase of RLUC-ATG8a/FLUC and RLUC-NBR1/FLUC ratios normalized to mock, suggesting reduced autophagic turnover (Fig. 1A). This is the first indication that *Xanthomonas* infection blocks autophagic turnover *in planta*. To support our data from the quantitative dual-luciferase flux assay we monitored autophagosome formation using RFP-ATG8G that decorates autophagosomes (18). We infected *N. benthamiana* plants transiently expressing RFP-ATG8G with *Xcv ΔxopQ* and monitored the formation of autophagosomes in the presence or absence of Concanamycin A (ConA). ConA is an inhibitor of vacuolar acidification that blocks autophagic body degradation (35, 36). In the absence of ConA, *Xcv ΔxopQ* induced massive accumulation of autophagosome-like structures which could not be further enhanced by the presence of ConA (Fig. 1B). This confirmed our finding that *Xcv* modulates autophagic degradation *in planta*. The induction of autophagosome formation and suppression of autophagic degradation prompted us to investigate host autophagy by immunoblotting for endogenous ATG8 and Joka2 in *N. benthamiana* (16, 35). Joka2 protein abundance increased during infection, to a small extent 1-day post-inoculation (dpi), and to a greater extent at 2 dpi, while ATG8 protein levels only slightly increased at 2 dpi (Fig. 1C). Another indicator of impaired autophagy is the increased gene expression of the autophagic markers (36). Transcript levels of *Joka2*, *NbATG8-2.1/2* and *NbATG8-1.1/2* were significantly higher compared to mock infection at 2 dpi (Fig. 1D), with *NbATG8-2.1/2* showing an earlier

increase than the two other genes. To assess the relevance of suppressed autophagic degradation during infection, we determined bacterial growth in plants transiently expressing the autophagy suppressor AIMp. At 6 dpi, *Xcv* growth was significantly elevated in *N. benthamiana roq-1* plants (37) transiently expressing RFP-AIMp compared to empty vector (EV) control (Figure 1E). The same trend was observed when *ATG7* was silenced using virus-induced gene silencing (VIGS) in *N. benthamiana* as silencing of *ATG7* rendered plants more susceptible to *Xcv* Δ*xopQ* at 6 dpi (Fig. S1). Because T3Es were previously shown to modulate proteasome function and autophagy (18, 24, 26, 38), we also analyzed the autophagy responses to a nonpathogenic type-III secretion system (T3SS) mutant *Xcv ΔhrcN*, which is unable to drive secretion of T3Es (39). In contrast to *Xcv ΔxopQ*, the T3SS-deficient mutant *Xcv ΔhrcN* did not alter the RLUC-ATG8a/FLUC or RLUC-NBR1/FLUC ratio, nor protein abundance of ATG8 and Joka2 (Fig. S2A and B). Consistent with this, gene expression analysis also revealed no significant induction of the autophagy marker genes *Joka2* and *NbATG8-1.1/2* (Fig S2C). Together, these data support the model that *Xcv* blocks autophagy in a T3E-dependent manner to promote virulence.

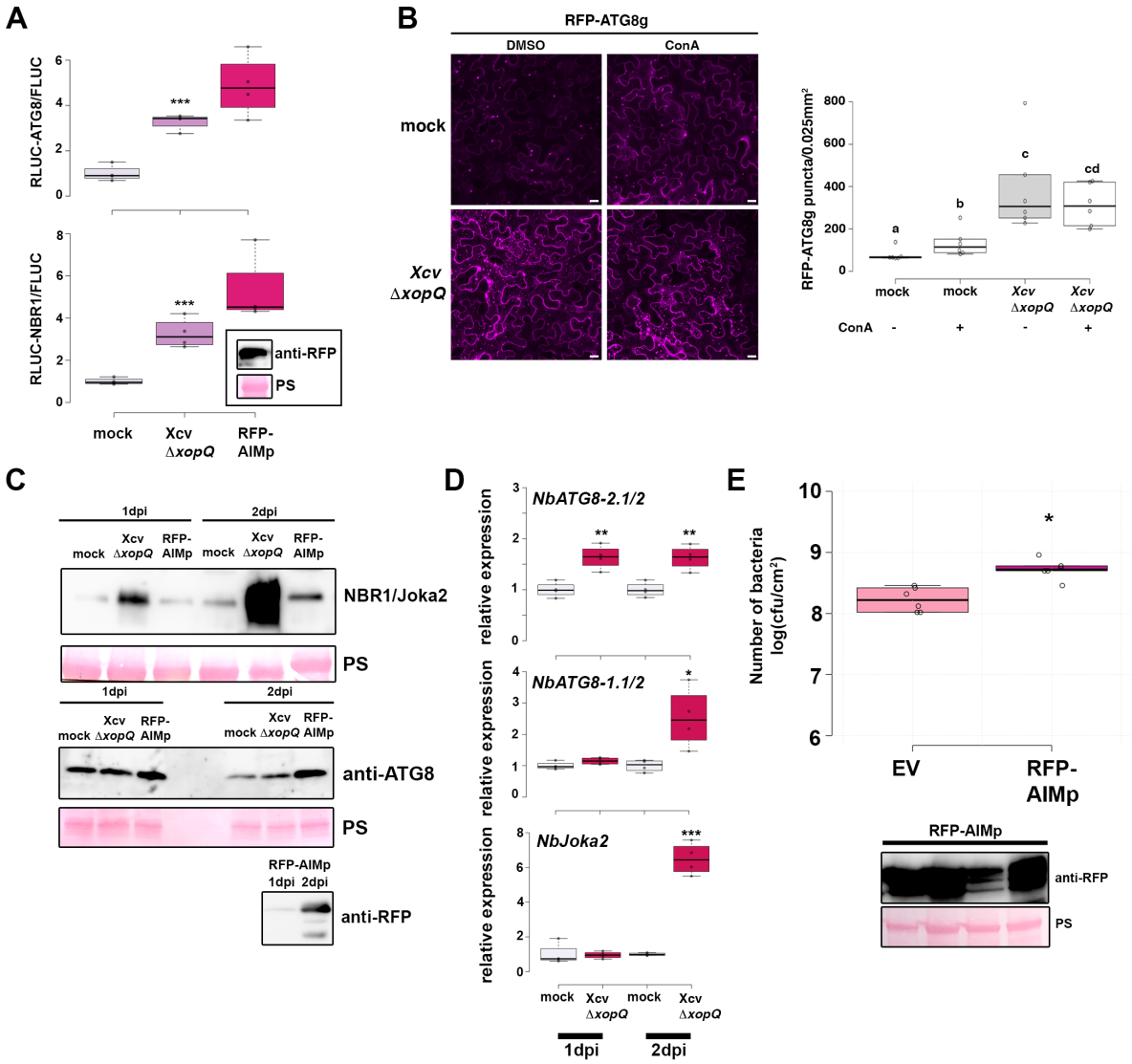

Figure 1: Xanthomonas blocks autophagy to enhance its pathogenicity

(A) Autophagic flux determined by quantitative dual-luciferase assay. RLUC-ATG8a or RLUC-NBR1 constructs were coexpressed with internal control FLUC in *N. benthamiana*. *Xcv ΔxopQ* was co-infiltrated with Agrobacteria containing the Luciferase constructs. Coexpression

178 of RFP-AIMp serves as a control for autophagy inhibition. Expression of the latter was
179 confirmend with western blot (inset). Renilla (RLUC) and Firefly (FLUC) luciferase activities
180 were simultaneously measured in leaf extracts at 48 h post- infiltration using the dual-luciferase
181 system. Values represent the mean ratio of RLUC-ATG8a and FLUC activities and error bars
182 show SD (n=4). Statistical significance (***P<0.001) was revealed by Student's t-test. The
183 experiment was repeated more than 3 times with similar results.
184 **(B)** RFP-ATG8g-labeled autophagosomes were quantified from plants infected with mock or
185 Xcv *ΔxopQ* at 2 dpi in the presence or absence of ConA (bars = 20 µm). Puncta were calculated
186 Puncta were calculated from z-stacks (15) of n=6 individuals using ImageJ. Center lines show
187 the medians; box limits indicate the 25th and 75th percentiles as determined by R software;
188 whiskers extend 1.5 times the interquartile range from the 25th and 75th percentiles and data
189 points are plotted as open circles. Different letters indicate statistically significant differences
190 (P < 0.05) as determined by one way ANOVA. The experiment was repeated twice with similar
191 results.
192 **(C)** Immunoblot analysis of NBR1 and ATG8 protein levels in Xcv *ΔxopQ* or mock infected
193 *N. benthamiana* plants at 1 and 2dpi. Agrobacterium-mediated transient expression of RFP-
194 AIMp serves as a control for autophagy suppression. Ponceau Staining (PS) served as a loading
195 control. The experiment was repeated three times with similar results.
196 **(D)** RT-qPCR analysis of *NbATG8-1.1/2, NbATG8-2.1/2* and *NbJoka2* transcript levels upon
197 challenge of *N. benthamiana* plants with Xcv *ΔxopQ* for 1 and 2 dpi compared to mock infected
198 plants. Values represent mean + SD (n=4) relative to mock control of respective time point and
199 were normalized to *PP2A*. Statistical significance (*P < 0.05, **P < 0.01, *** P < 0.001) was
200 revealed by Student's t-test.
201 **(E)** Bacterial density in leaves of *N. benthamiana* infected with Xcv *ΔxopQ* in the presence or
202 absence autophagy suppressor RFP-AIMp. Leaves were syringe infiltrated with OD_{600} =
203 0.0004, and colony-forming units were counted at 6 dpi. Compared to empty vector control
204 (EV), AIMp expressing plants (n=6) harbour significantly more bacteria. Statistical
205 significance (*P < 0.05) was revealed by Student's t-test. Expression of RFP-AIMp was
206 verified at 6 dpi with an anti-RFP blot (n=4).
207
208 ***T3E XopL suppresses autophagy***
209 To address which T3E(s) might manipulate autophagy, we used the quantitative dual-luciferase
210 autophagy assay. We screened for *Xcv* T3Es XopJ, XopD and XopL with known function in
211 proteolytic degradation pathways (28, 40-43) as well as XopS which has not been described to
212 degradation machineries. Measurement of luciferase activities showed that the transient
213 expression of XopL, a previously characterized E3 ligase (41), led to a significant increase in
214 RLUC-ATG8a/FLUC and RLUC-NBR1/FLUC ratio (Fig. 2A), which was consistent across
215 multiple experiments. In contrast, transient expression of XopD and XopS had no evident effect
216 in the luciferase assay, while XopJ also significantly impacted autophagy (Fig. S3A). This may
217 be due to its inhibitory effect on the proteasome (38), as MG132 (a proteasome inhibitor)
218 treatment also results in an increase of the RLUC-ATG8a/FLUC ratio (Fig S3B). Performing
219 immunoblot analysis of ATG8 protein levels in *N. benthamiana* leaves, we found that transient
220 expression of XopL resulted in an accumulation of NBR1 and ATG8 proteins. This could not
221 be further increased by ConA treatment in the case of ATG8 (Fig. 2B and C).
222 To validate that XopL also acts as an autophagy suppressor during *Xcv* infection we constructed
223 a *xopL* deletion mutant in *Xcv ΔxopQ*. The deletion mutant displayed reduced growth and
224 symptom development upon infection of tomato plants and in *N. benthamiana* (Fig S4),
225 demonstrating that XopL is an essential virulence factor. Utilizing our quantitative dual-
226 luciferase autophagy assay, we discovered that *Xcv ΔxopQ ΔxopL* was unable to suppress
227 autophagy to levels observed in tissues infected with *Xcv ΔxopQ* levels (Fig. 2D), indicating
228 that XopL has a major impact on autophagy during infection. However, *Xcv ΔxopQ ΔxopL* still

leads to a slight increase in both RLUC-ATG8a/FLUC and RLUC-NBR1/FLUC ratios, suggesting that *Xcv* possesses another T3E with a redundant function. By analyzing ATG8 and NBR1 protein levels, we also verified that XopL partially contributes to an increase in ATG8 and NBR1 accumulation (Fig. 2E), supporting the notion that XopL suppresses autophagic degradation during infection. To analyze whether XopL has similar functions in other plant species, we generated transgenic *Arabidopsis thaliana* lines expressing GFP-XopL under the UBQ10 promoter. Confocal microscopy analysis revealed that GFP-XopL localizes to punctate structures in *A. thaliana* leaf epidermal cells (Fig. S5C). Further analysis of GFP-XopL transgenic *A. thaliana* plants revealed that NBR1 protein abundance in the absence and presence of ConA treatment is drastically increased (Fig. S5A), suggesting a block of NBR1 turnover. The early senescence phenotype of transgenic lines expressing XopL (Fig. S5B) and elevated gene expression of ATG8a and NBR1 is also indicative of altered autophagy responses (Fig. S5D).

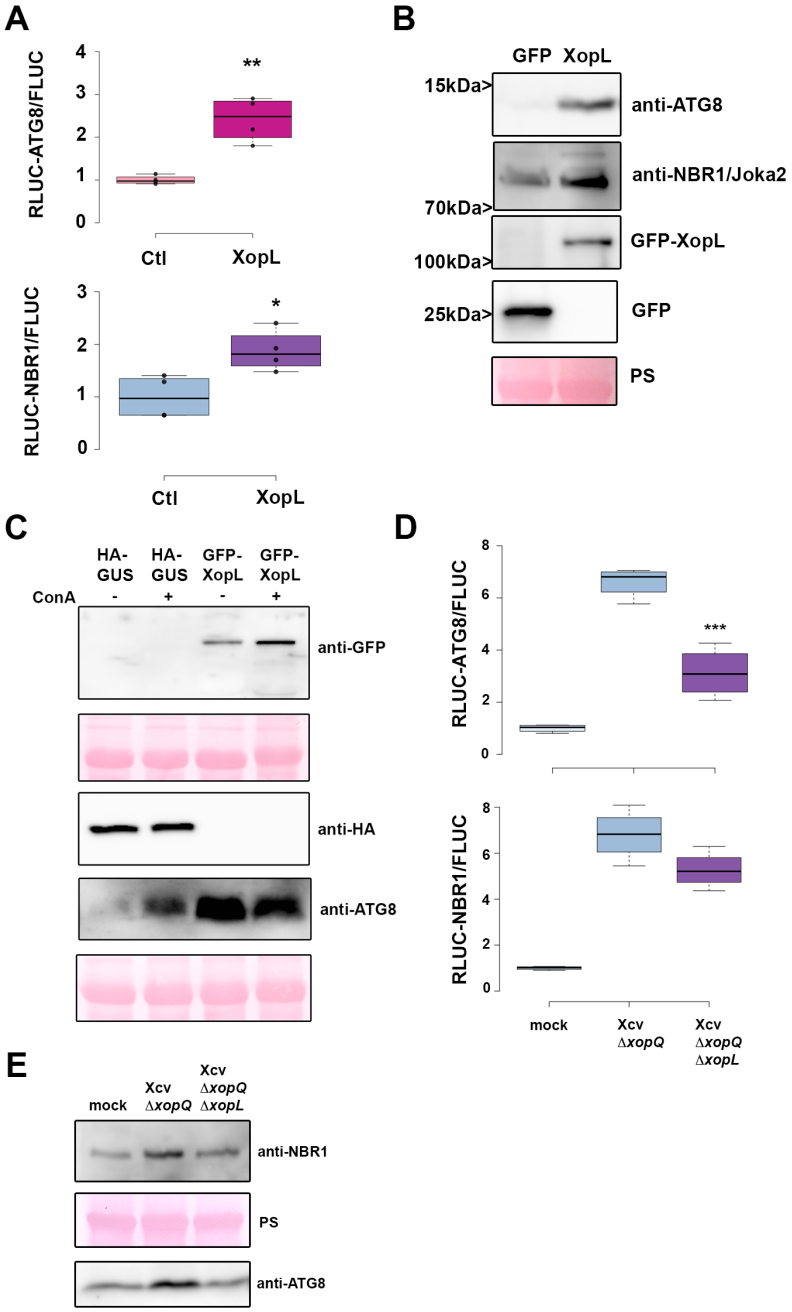

Figure 2: Xanthomonas T3E XopL is suppressing autophagy

(A) RLUC-ATG8a or RLUC-NBR1 constructs were coexpressed with internal control FLUC in *N. benthamiana*. XopL or control (Ctl) constructs were co-infiltrated. RLUC and FLUC activities were simultaneously measured in leaf extracts at 48 h post- infiltration using the dual-luciferase system. Values represent the mean ratio of RLUC-ATG8a and FLUC activities and error bars show SD (n=4). Statistical significance (* $P < 0.5$, ** $P < 0.01$) was revealed by Student's *t*-test. The experiment was repeated more than 3 times by 2 different people with similar results.
(B) Immunoblot analysis of NBR1 and ATG8 protein levels in *N. benthamiana* plants transiently expressing GFP-XopL or GFP control at 2dpi. Expression of GFP-XopL and GFP were verified with an anti-GFP antibody. Ponceau Staining (PS) served as a loading control. T The experiment was repeated at least three times by 2 different people with similar results.
(C) Immunoblot analysis of NBR1 and ATG8 protein levels in *N. benthamiana* plants transiently expressing XopL or GUS control at 2dpi in the presence or absence of ConA. Expression of GFP-XopL was verified with an anti-GFP antibody, while expression of GUS-HA was confirmed with an anti-HA antibody. Ponceau Staining (PS) served as a loading control. The experiment was repeated twice with similar results.
(D) RLUC-ATG8a or RLUC-NBR1 constructs were coexpressed with internal control FLUC in *N. benthamiana*. Xcv *ΔxopQ and* Xcv *ΔxopQ ΔxopL* were co-infiltrated with Agrobacteria containing the respective constructs. RLUC and FLUC activities were simultaneously measured in leaf extracts at 48 h post- infiltration using the dual-luciferase system. Values represent the mean ratio of RLUC-ATG8a and FLUC activities and error bars show SD (n=4). Statistical significance (***$P < 0.001$) was revealed by Student's *t*-test. The experiment was repeated 3 times with similar results.
(E) Immunoblot analysis of NBR1 and ATG8 protein levels in Xcv *ΔxopQ,* Xcv *ΔxopQ ΔxopL* or mock infected *N. benthamiana* plants at 2dpi. Ponceau Staining (PS) served as a loading control. The experiment was repeated twice with similar results.

NBR1/Joka2-mediated selective autophagy degrades ubiquitinated XopL

Our findings demonstrate that *Xcv* not only blocks bulk autophagy but also NBR1/Joka2-dependent selective autophagy. Previous studies imply that NBR1/Joka2 mediates xenophagy by degrading viral particles and that Joka2 is required for immunity against bacteria and *Phytophthora* (16, 18, 20, 44). Plant NBR1 is a hybrid of the mammalian autophagy adaptors NBR1 and p62/SQSTM1 (35). The latter was shown to mediate xenophagy of *Mycobacterium tuberculosis* (Mtb) by binding to the Mtb ubiquitin-binding protein Rv1468c and ubiquitin-coated *Salmonella enterica* in human cells (45, 46). However, the mode of action and targets of plant NBR1 during microbial infection remain elusive. Revisiting our previous results, we realized that the abundance of XopL increased when we blocked vacuolar degradation with ConA (Fig. 2C), which is also true for *A. thaliana* plants stably expressing XopL (Fig S5A) or *N. benthamina* leaves expressing both XopL and the autophagy suppressor AIMp (Fig. 3A). To further validate if XopL undergoes autophagic degradation in the vacuole, we used a transgenic line *A. thaliana* expressing GFP-XopL treated with ConA to block vacuolar turnover. Confocal microscopy was performed in root cells as vacuolar degradation is easier to assess in this tissue. We observed multiple GFP-labeled structures reminiscent of autophagic bodies in root vacuoles of ConA-treated seedlings compared to the control (Fig. S6). As autophagic degradation of viral proteins and animal pathogenic bacteria is mediated by NBR1, we decided to examine whether XopL and NBR1 associate *in planta*. Intriguingly, we discovered that XopL co-localizes with NBR1 in puncta and in large aggregate-like structures (Fig. 3B), suggesting that NBR1 associates with XopL *in planta*. Association of both proteins was determined using Förster resonance energy transfer by fluorescence lifetime imaging microscopy (FRET-FLIM). Only in the presence of RFP-XopL a significant reduction of 0.1 ns in the lifetime of the donor Joka2 was observed in comparison to co-expression of RFP or donor alone (Fig. 3C). These findings

295 prompted us to investigate whether XopL might be targeted by NBR1/Joka2 for autophagic
296 degradation, similar to insoluble ubiquitinated protein aggregates (47). Performing pull-down
297 experiments with GFP-XopL, we discovered that XopL associates with NBR1/Joka2 *in planta*
298 (Fig. 3D), confirming the results of our co-localization study. To address whether E3 ligase
299 activity of XopL is required for interaction, we employed the triple point mutant of $XopL_{H584A}$
300 $_{L585A\ G586E}$ (hereafter referred to as XopL ΔE3), lacking E3 ligase activity (41, 54). Co-IP
301 experiments revealed that XopL ΔE3 was also able to pull-down NBR1/Joka2 after transient
302 expression in *N. benthamiana* (Fig. 3E). This suggests that NBR1/Joka2 may not mediate the
303 degradation of a complex containing XopL and its ubiquitinated target protein(s), but rather
304 targets XopL for autophagic degradation. Given the fact that XopL is degraded by autophagy
305 and associates with NBR1/Joka2, we next analyzed stability of XopL in Joka2 silenced *N.*
306 *benthamiana* plants. Silencing of NBR1/Joka2 was confirmed by qPCR (Fig. S7). Indeed, we
307 could observe an increase in XopL protein abundance in pTRV2-Joka2 plants (Fig. 3F), arguing
308 for a direct participation of NBR1/Joka2 in XopL turnover. To assess whether this might impact
309 pathogenicity of *Xcv* we performed bacterial growth assays using the pTRV2-Joka2 plants.
310 Increased growth at 3 dpi and 6dpi of *Xcv ΔxopQ* in *N. benthamiana* plants silenced for Joka2
311 strengthened our finding that Joka2 is having anti-bacterial effects on *Xcv ΔxopQ* (Fig. 3G). As
312 NBR1/Joka2 or p62 recognize their cargos by their ability to bind ubiquitinated substrates, we
313 hypothesized that XopL might be ubiquitinated *in planta*. To test this, we transiently expressed
314 GFP-XopL in *N. benthamiana* leaves and then immunoprecipitated GFP-XopL from leaf
315 protein extracts. Ubiquitinated GFP-XopL was detected using immunoblotting and anti-
316 ubiquitin sera. GFP-XopL, but not the GFP control, displayed polyubiquitination *in planta*,
317 while GFP-XopL ΔE3 showed reduced polyubiquitination (Fig. 3H). To further confirm the
318 ubiquitination of XopL, we purified total ubiquitinated proteins using the ubiquitin pan selector,
319 which is based on a high-affinity single domain antibody that is covalently immobilized on
320 cross-linked agarose beads. Since XopL is stabilized by the autophagy suppressor AIMp, we
321 co-expressed XopL together with AIMp. We detected a faint smear of high-molecular weight
322 XopL, which was strongly enhanced when co-expressed with AIMp but absent in the GFP
323 control (Fig. 3I). To identify ubiquitinated residues within the XopL protein, we
324 immunoprecipitated GFP-XopL from *N. benthamiana* leaves transiently expressing GFP-XopL
325 and performed mass spectrometry (MS) analysis. *In planta* MS analysis revealed one potential
326 ubiquitination site at lysine 191 (K191) in the N-terminal part of XopL (Fig. S8). For plant E3
327 ligases such as PUB22, it has been reported that its stability is dependent on its
328 autoubiquitination activity (48). Using MBP-XopL in an *in vitro* ubiquitination assay we
329 confirmed self-ubiquitination (Fig. S9A), indicated by the presence of higher molecular weight
330 bands probing with an anti-MBP. Preforming LC-MS/MS we did detect the same ubiquitination
331 (K191) site identified *in planta* when we analyzed *in vitro* ubiquitination samples containing
332 GST-XopL (Fig. S9B). This strongly argues for an autoubiquitination of XopL. However, we
333 cannot rule out trans-ubiquitination by plant E3 ligases, as XopL ΔE3 still interacts with NBR1
334 and is still ubiquitinated in *planta*, although to a lesser extent. This is strengthened by our
335 findings showing that the mutation of lysine 191 to alanine (K191A) rendered the XopL K191A
336 more stable than WT XopL (Fig. 3J) without altering its subcellular localization (Fig. S10) but
337 did not abolish ubiquitination of XopL and association with NBR1/Joka2 (Fig. 3K, Fig. S11).
338 This might indicate the presence of additional ubiquitination sites in XopL. Taken together, our
339 results suggest that XopL is ubiquitinated *in planta* and subjected for NBR1/Joka2-dependent
340 selective autophagy.
341
342
343
344
345

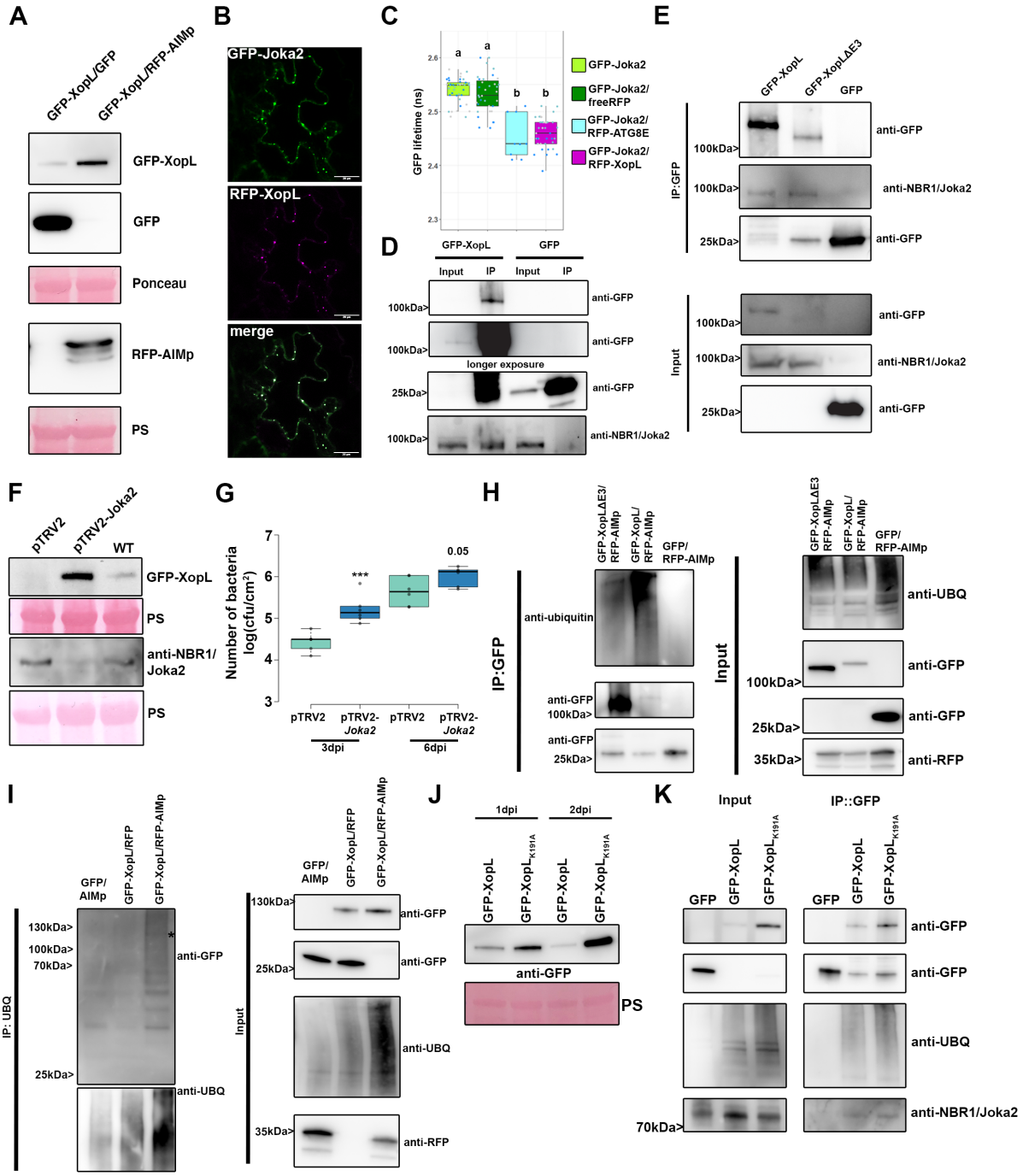

Figure 3: XopL is ubiquitinated in planta and degraded by NBR1-mediated selective autophagy

(A) Autophagy suppression enhances XopL stability. GFP-XopL was coexpressed with GFP or RFP-AIMp. Proteins were separated by SDS-PAGE and detected by immunoblotting using the indicated antibodies. Ponceau Staining (PS) served as a loading control. The experiment was repeated three times by two different people with similar results.

(B) Colocalization of GFP-XopL with RFP-Joka2 in *N. benthamiana* leaves. Imaging was performed 2 d after transient expression and images represent single confocal planes from abaxial epidermal cells (bars = 20 µm). The experiment was repeated twice with similar results.

(C) FRET FLIM measurements of GFP-Joka2 and RFP-XopL in *N. benthamiana* leaves. The freeRFP construct served as a negative control and RFP-ATG8E (n = 9) as a positive control. Scattered points show individual data points, color indicates biological repeats. The lifetime (in ns) of GFP-Joka2 (donor, n = 41) was significantly reduced in the presence of RFP-XopL (n =

360 40) but not in the presence of freeRFP (n = 35). Significant differences were calculated using
361 Wilcoxon rank sum test. The experiment was repeated three times with similar results.
362 **(D)** Immunoprecipitation (IP) of GFP-XopL reveals association with NBR1. Immunoblots of
363 input and IP samples from *N. benthamiana* plants transiently expressing GFP or GFP-XopL
364 were probed with anti-GFP and anti-NBR1 antibodies.
365 **(E)** Immunoprecipitation (IP) of GFP-XopL and GFP-XopL ΔE3 reveals association with
366 NBR1. Immunoblots of input and IP samples from *N. benthamiana* plants transiently
367 expressing GFP, GFP-XopL and GFP-XopL ΔE3 were probed with anti-GFP and anti-NBR1
368 antibodies.
369 **(F)** Stability of XopL is increased in Joka2 silenced plants. GFP-XopL was transiently
370 expressed in pTRV2, pTRV2-Joka2 and *N. benthamiana* WT plants. Expression of binary
371 constructs was verified with an anti-GFP antibody. Joka2 silencing was verified using an anti-
372 NBR1 antibody. Ponceau Staining (PS) served as a loading control. The experiment was
373 repeated twice with similar results.
374 **(G)** Growth of Xcv *ΔxopQ* in *N. benthamiana* plants silenced for *Joka2* (pTRV2-Joka2)
375 compared to control plants (pTRV2). Leaves were dip-inoculated with a bacteria suspension at
376 OD_{600} = 0.2. and bacteria were quantified at 3 and 6 dpi. Data represent the mean SD (n = 6).
377 Significant differences were calculated using Student's *t-test* and are indicated by: ***, $P <$
378 0.001. The experiment was repeated three times with similar trends.
379 **(H)** XopL is ubiquitinated *in planta*. GFP-XopL, GFP-XopL ΔE3 were transiently expressed
380 in *N. benthamiana*. RFP-AIMp was co-infiltrated to stabilize both XopL variants. Samples were
381 taken 48 hpi, and total proteins (Input) were subjected to immunoprecipitation (IP) with GFP-
382 Trap beads, followed by immunoblot analysis of the precipitates using either anti-GFP or anti-
383 ubiquitin antibodies. GFP served as a negative control. RFP-AIMp expression was verified by
384 an anti-RFP antibody. The experiment was repeated three times with similar results.
385 **(I)** XopL is ubiquitinated *in planta*. GFP-XopL was transiently expressed in *N. benthamiana*.
386 RFP-AIMp was co-infiltrated to stabilize GFP-XopL. Samples were taken 48 hpi, and total
387 proteins (Input) were subjected to immunoprecipitation (IP) with the ubiquitin pan selector,
388 followed by immunoblot analysis of the precipitates using either anti-GFP or anti-ubiquitin
389 antibodies. GFP served as a control. RFP-AIMp expression was verified by an anti-RFP
390 antibody. Asterisk indicates the GFP-XopL full-length protein. The experiment was repeated
391 three times with similar results.
392 **(J)** Immunoblot analysis GFP-XopL and GFP-$XopL_{K191A}$ at 1 and 2 dpi using an anti-GFP
393 antibody. Ponceau Staining (PS) served as a loading control. The experiment was repeated three
394 times by two different people with similar results.
395 **(K)** Mutation of Lysin 191 does not abolish poly-ubiquitination of XopL and association with
396 NBR1. GFP-XopL and GFP-$XopL_{K191A}$ were transiently expressed in *N. benthamiana*. Samples
397 were taken 48 hpi, and total proteins (Input) were subjected to immunoprecipitation (IP) with
398 GFP-Trap beads, followed by immunoblot analysis of the precipitates using either anti-GFP,
399 anti-ubiquitin and anti-NBR1 antibodies. GFP served as a control. The experiment was repeated
400 three times with similar results.
401
402 ***XopL interacts with the autophagy component SH3P2 and degrades it via the proteasome to***
403 ***dampen autophagy***
404 Previously, XopL was characterized as a novel class of E3 ligases capable of suppressing plant
405 defense responses. However, its plant target(s) remained unknown (41). To analyze whether
406 XopL directly targets autophagy components to act as an autophagy suppressor, we carried out
407 a yeast-two hybrid (Y2H) screen using a cDNA library from tobacco (*Nicotiana tabacum*). Our
408 previous interactions studies indicate that the tobacco cDNA library is sufficient to identify host
409 targets of *Xcv* T3Es that are conserved across different plant species, such as pepper, tomato
410 and *A. thaliana* (38, 49, 50). One cDNA identified in the Y2H screening for XopL interacting

411 proteins encoded a homologue of *A. thaliana* SH3P2, with an identity of 74 % (Fig S11A).
412 Homologues are also present in *Nicotiana benthamiana* (NbSH3P2a and NbSH3P2b, 98%
413 identity) and tomato (SlSH3P2, 96% to NtSH3P2) (Fig S12A, B). Direct interaction assays in
414 yeast revealed that XopL is able to interact with SH3P2 from *N. tabacum* and *N. benthamiana*
415 (Fig. 4A and Fig. S12C). SH3P2 from *A. thaliana* was previously identified as a novel
416 autophagy component that interacts with ATG8 isoforms and binds to phosphatidylinositol 3-
417 phosphate (PI3P) to regulate autophagosome formation, having also a potential role in late
418 events of autophagy (51, 52). SH3P2 was also found to play a role in the recognition of
419 ubiquitinated membrane proteins, and in targeting them to the endosomal sorting complexes
420 required for transport (ESCRT) machinery (53). We next sought to determine whether the
421 interaction between XopL and SH3P2 occurs *in planta*. Due to expression problems of tobacco
422 SH3P2 and also due to their high identity, we conducted further interaction studies with
423 *At*SH3P2. Using bimolecular fluorescence complementation and in *vivo* co-
424 immunoprecipitation (co-IP), we found that XopL and *At*SH3P2 interact in the plant cell, in
425 punctate structures resembling autophagosomes (Fig. 4B and C; Supp Video 1). Additional *in*
426 *vitro* co-IP data, using *E. coli* produced recombinant MBP-XopL and GST-*At*SH3P2, suggests
427 that XopL and SH3P2 might directly interact with each other (Fig. 4D). Given the fact that
428 SH3P2 from *A. thaliana* interacts with ATG8 and XopL localizes in puncta within plant cells
429 (54), we assessed whether XopL co-localizes with autophagosomes *in planta*. We were able to
430 identify that transient expression of GFP-XopL in *N. benthamiana* with the autophagosome
431 markers RFP epitope tagged ATG8G, ATG8E and SH3P2 resulted in strong co-localization
432 (Fig. 4E). This further supports the idea that XopL is functioning in the autophagy pathway by
433 associating with these components *in planta*.
434 Our results so far suggest that XopL might manipulate autophagy by interacting with the
435 autophagy component AtSH3P2. Previous research on AtSH3P2 revealed that RNAi-mediated
436 downregulation of AtSH3P2 affects the autophagy pathway (51). Since XopL possesses E3
437 ligase activity, we next sought to investigate whether XopL might destabilize SH3P2 and
438 thereby block autophagic degradation. Indeed, *in planta* transient co-expression of XopL
439 (tagged either with GFP or HA) and AtSH3P2-GFP resulted in reduced SH3P2 protein
440 abundance in *N. benthamiana* (Fig. 4F). Degradation of AtSH3P2 by XopL was dependent on
441 a functional proteasome, as chemical inhibition of the proteasome with MG132 partially
442 restored AtSH3P2-GFP protein levels (Fig. 4G). To assess whether this was directly mediated
443 by XopL and its E3 ligase activity, we performed an *in vitro* ubiquitination assay. In the
444 presence of all required components of the E1-E2-E3 system, we observed that GST-XopL
445 ubiquitinated MBP-AtSH3P2, which is indicated by a laddering pattern, leading to larger sized
446 molecular species of MBP-AtSH3P2, when probed with the anti-MBP antibody (Fig. 4H).
447 These results indicate that the E3 ligase activity of XopL might be crucial in the SH3P2-
448 dependent modulation of host autophagy. To address this, we employed the XopL ΔE3 mutant,
449 lacking E3 ligase activity (41, 54). Transient co-expression of XopL ΔE3 together with SH3P2
450 revealed that XopL requires its E3 ligase activity to trigger the degradation of AtSH3P2 in *N.*
451 *benthamiana* (Fig. 4I). This was not due to an altered localization of XopL ΔE3, as it still co-
452 localizes with AtSH3P2 upon transient expression in *N. benthamiana* (Fig. S13). As a
453 consequence of not being able to degrade SH3P2 *in planta*, XopL ΔE3 did not lead to a
454 suppression of autophagy responses in the quantitative luciferase autophagy assay and increase
455 in ATG8 protein levels (Fig. 4J and K). Immunoblot analysis also revealed that XopL ΔE3 is
456 more unstable compared to XopL WT and also degraded by autophagy, as it is not able to block
457 autophagy (Fig S14). Taken together, our findings support the notion that the E3 ligase activity
458 of XopL as well as its ability to directly ubiquitinate and degrade AtSH3P2 promote suppression
459 of autophagy.
460
461

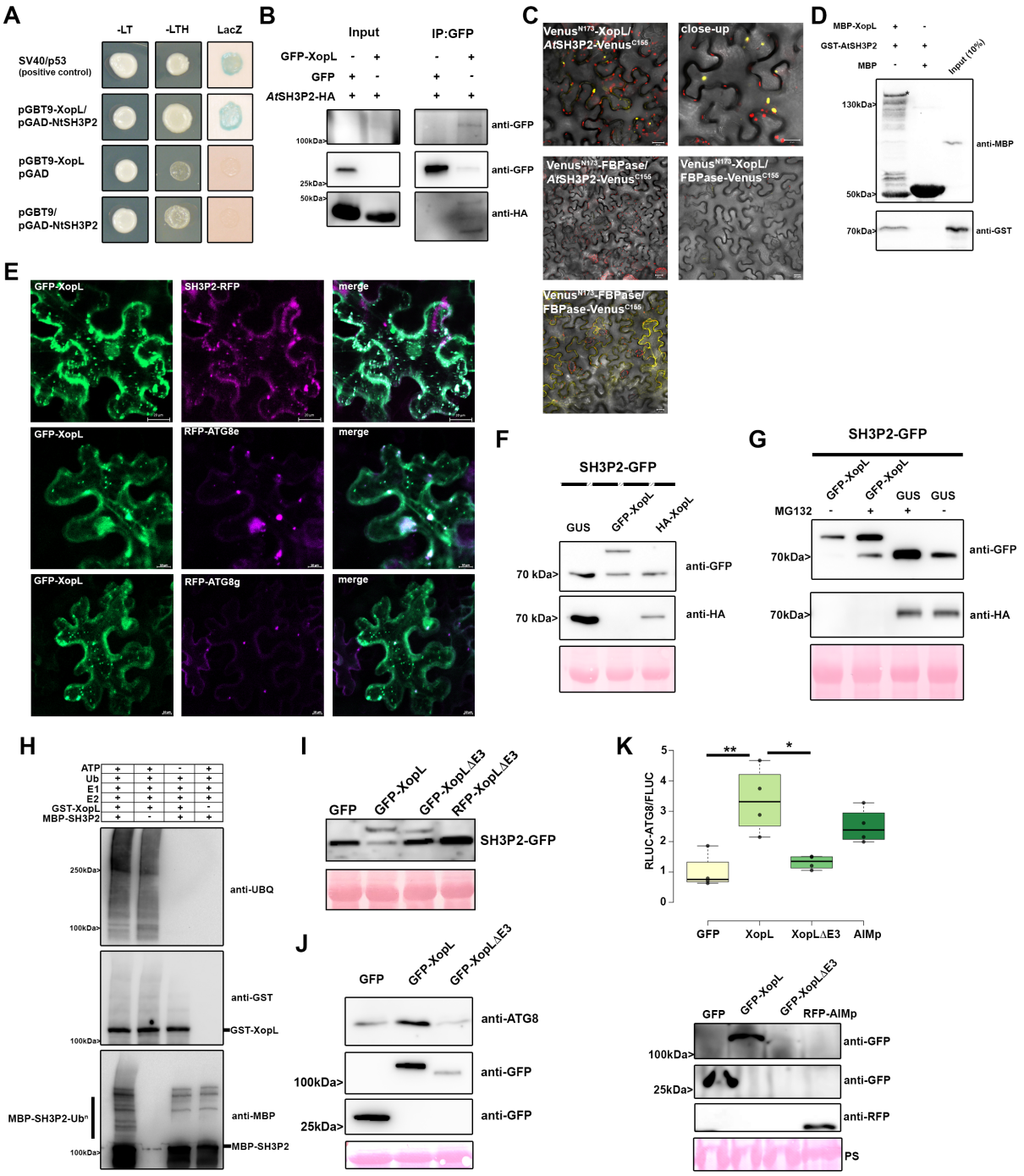

Figure 4: XopL interacts with SH3P2 and mediates its proteasome degradation via its E3 ligase activity to block autophagy

(A) Interaction of XopL with SH3P2 in yeast two-hybrid assays. XopL fused to the GAL4 DNA-binding domain was expressed in combination with SH3P2 fused to the GAL4 activation domain (AD) in yeast strain Y190. Cells were grown on selective media before a LacZ filter assay was performed. pSV40/p53 served as positive control, while the empty AD or BD vector served as negative control. NtSH3P2 = *Nicotiana tabacum* SH3P2. –LT = yeast growth on medium without Leu and Trp, –HLT = yeast growth on medium lacking His, Leu, and Trp, indicating expression of the HIS3 reporter gene. LacZ, activity of the lacZ reporter gene.

(B) Coimmunoprecipitation of GFP-XopL with AtSH3P2-HA. GFP-XopL or GFP were transiently coexpressed with AtSH3P2-HA in leaves of *N. benthamiana*. After 48 h, total proteins (Input) were subjected to immunoprecipitation (IP) with GFP-Trap beads, followed by

475 immunoblot analysis using either anti-GFP or anti-HA antibodies. AtSH3P2 = *Arabidopsis*
476 *thaliana* SH3P2. Two repetitions with similar results have been conducted.
477 **(C)** Visualization of protein interactions *in planta* by the bimolecular fluorescence
478 complementation assay. Yellow fluorescent protein (YFP) confocal microscopy images show
479 *Nicotiana benthamiana* leaf epidermal cells transiently expressing $Venus^{N173}$-XopL in
480 combination with AtSH3P2-$Venus^{C155}$. A positive control showing the dimerization of
481 fructose-1,6-bisphosphatase (FBPase) within the cytosol. The combination of $Venus^{N173}$-XopL
482 with FBPase-$Venus^{C155}$ or $Venus^{N173}$-FBPase with AtSH3P2-$Venus^{C155}$ do not induce YFP
483 fluorescenc and serve as negative controls. Bars = 20 µm. AtSH3P2 = *Arabidopsis thaliana*
484 SH3P2. The experiment has been repeated twice with similar results.
485 **(D)** *In vitro* co-IP assay showing direct interaction of XopL with AtSH3P2. MBP-XopL and
486 GST-AtSH3P2 were expressed in E. coli. Pull down was performed using amylose resin.
487 Proteins were detected in an immunoblot using antibodies as indicated.
488 **(E)** Colocalization analysis of GFP-XopL with SH3P2-RFP, RFP-ATG8e and RFP-ATG8g in
489 *N. benthamiana* leaves. Imaging was performed 2 d after transient expression and images
490 represent single confocal planes from abaxial epidermal cells (scale bars = 20 µm and 10 µm,
491 lower panel). The experiment was repeated twice with similar results.
492 **(F)** Total proteins were extracted 48 hpi with *A. tumefaciens* harboring the respective GFP-
493 XopL, HA-XopL and SH3P2-GFP expression constructs. SH3P2-GFP protein levels (lower
494 band) were detected using an anti-GFP antibody. Expression of the XopL was verified using an
495 anti-HA or anti-GFP antibody. Expression of GUS-HA served as a control. Ponceau S staining
496 serves as a loading control. The experiment was repeated three times with similar results.
497 **(G)** SH3P2-GFP was transiently coexpressed together with GUS-HA and GFP-XopL in *N.*
498 *benthamiana* using agroinfiltration. At 42 hpi, 200 mM MG132 was infiltrated into *A.*
499 *tumefaciens*-inoculated leaves, and leaf material was collected 48 hpi. Expression of SH3P2-
500 GFP (lower band) and GFP-XopL (upper band) was detected using an anti-GFP antibody. GUS-
501 HA expression was confirmed with an anti-HA antibody. Ponceau S staining serves as a loading
502 control. The experiment was repeated three times with similar results.
503 **(H)** *In vitro* ubiquitination assay reveals ubiquitination of SH3P2 by XopL. GST-XopL, and
504 MBP-SH3P2 were tested using the Arabidopsis His-AtUBA1 and His-AtUBC8. Lanes 2 to 4
505 are negative controls. Proteins were separated by SDS-PAGE and detected by immunoblotting
506 using the indicated antibodies. The experiment was repeated twice with similar results.
507 **(I)** SH3P2-GFP was transiently coexpressed together with GFP, GFP-XopL, GFP-XopL ΔE3
508 and RFP-XopL ΔE3 in *N. benthamiana* using agroinfiltration. GFP protein levels were detected
509 with an anti-GFP antibody. Ponceau S staining serves as a loading control. The experiment was
510 repeated three times with similar results.
511 **(J)** Immunoblot analysis of ATG8 protein levels in *N. benthamiana* plants transiently
512 expressing GFP-XopL, GFP-XopL ΔE3 or GFP control at 2dpi. Expression of binary constructs
513 was verified with an anti-GFP antibody. Ponceau Staining (PS) served as a loading control. The
514 experiment was repeated twice with similar results.
515 **(K)** RLUC-ATG8a constructs were coexpressed with internal control FLUC in *N. benthamiana*.
516 GFP-XopL, GFP-XopL ΔE3 or GFP control were co-infiltrated together with RLUC/FLUC
517 mixture. *Renilla* and *Firefly* luciferase activities were simultaneously measured in leaf extracts
518 at 48 hpi using the dual-luciferase system. Values represent the mean ratio of RLUC-ATG8a
519 and FLUC activities and error bars show SD (n=4). Statistical significance (* $P < 0.5$, ** $P <$
520 0.01) was revealed by Student's *t*-test. The experiment was repeated 3 times by 2 different
521 people with similar results. Expression of proteins was verified with indicated antibodies.
522
523 ***SH3P2 is required for autophagy and immunity against Xcv in N. benthamiana***
524 Previously, downregulation of SH3P2 is *A. thaliana* has been shown to reduce autophagic
525 activity (51). However, the role of SH3P2 is still controversial, as another study identified that

526 SH3P2 functions in clathrin-mediated endocytosis without having any obvious effects on dark-
527 induced autophagy (53). To shed light on the enigmatic and versatile function of SH3P2, we
528 used virus-induced gene silencing (VIGS) in *N. benthamiana* targeting both *NbSH3P2a* and *b*.
529 Silencing had no obvious effect on plant growth and silencing efficiency was assessed by qPCR
530 (Fig. S15A and B). Subsequent immunoblot analysis revealed that in comparison to the pTRV2-
531 GFP control, SH3P2 VIGS plants displayed accumulation of ATG8 protein levels, similar
532 results to that reported by Zhuang et al. 2013 (Fig. 5A). To corroborate this finding, we
533 transiently expressed GFP-ATG8e in control and silenced plants and monitored autophagosome
534 formation upon AZD8055 treatment, a TOR inhibitor and autophagy activator. The number of
535 autophagosomes increased upon AZD8055 treatment in both plants but were significantly less
536 in SH3P2 VIGS plants when treated with ConA (Fig. 5B and C). This indicates that
537 downregulation of SH3P2 in *N. benthamiana* impairs maturation of autophagosomes and hence
538 autophagic degradation. Indeed, using confocal microscopy of GFP-ATG8E, we observed
539 aberrant autophagosomal structures in VIGS SH3P2 plants that might explain why autophagy
540 is not entirely functional anymore. These data suggest that SH3P2 might be required during
541 later steps as autophagosome induction seems to be normal during autophagy induction with
542 AZD8055. VIGS in *N. benthamiana roq1* plants and subsequent bacterial growth measurements
543 with *Xcv* and *Xcv ΔxopL* revealed that pTRV2-*SH3P2* plants are more susceptible towards *Xcv*
544 similar to pTRV2-*Joka2* plants (Fig. 5D). Essentially, reduced growth of *Xcv ΔxopL* was
545 rescued in both SH3P2 and Joka2 silenced plants strengthening our findings that XopL
546 suppresses both bulk and selective autophagy pathways to cause disease (Fig. 5D).

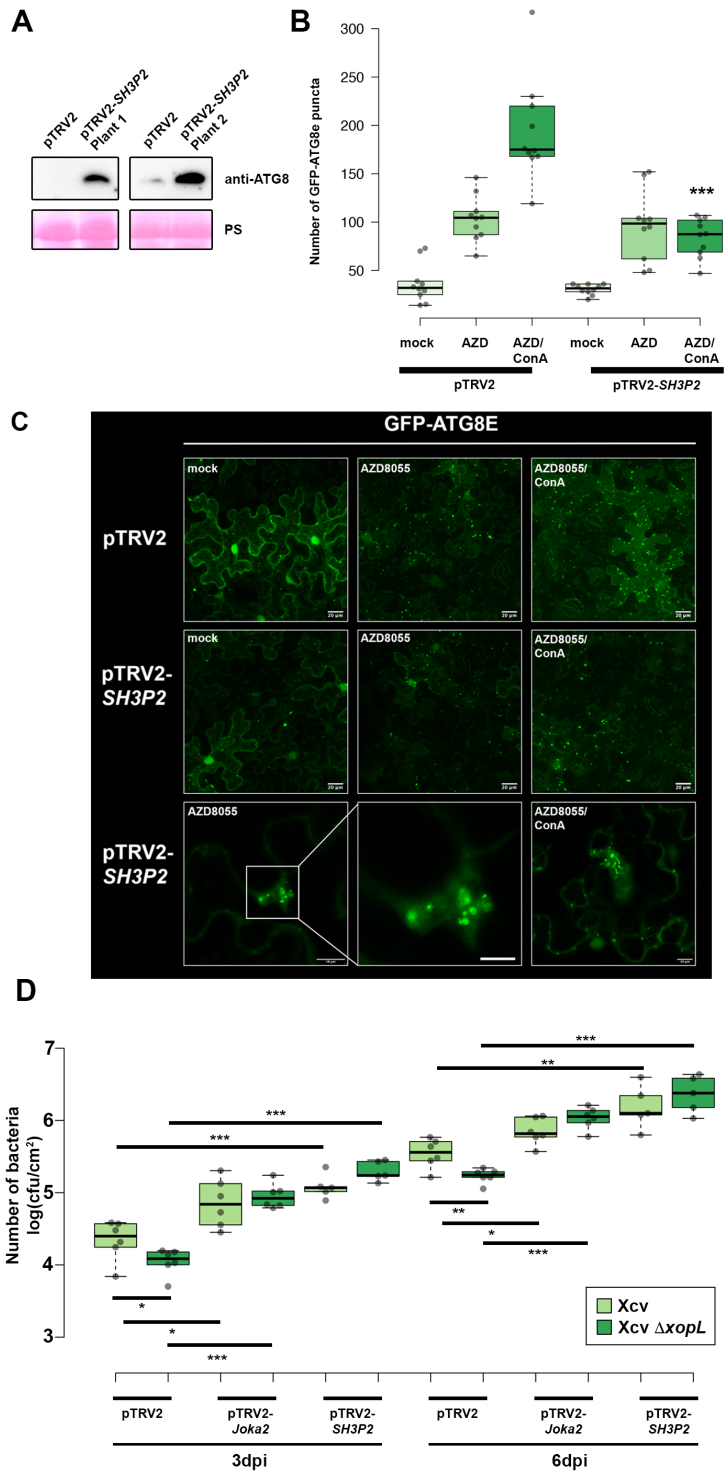

Figure 5: Silencing of SH3P2 suppresses autophagic degradation and is beneficial for *Xanthomonas* growth

(A) Immunoblot analysis of ATG8 protein levels in *N. benthamiana* pTRV2 (control) and pTRV2-*SH3P2* (*SH3P2* silencing) 2 weeks after VIGS. Ponceau Staining (PS) served as a loading control. The experiment was repeated twice with similar results.
(B) GFP-ATG8e-labeled autophagosomes were quantified from pTRV2 or pTRV2-SH3P2 plants transiently expressing GFP-ATG8e at 2dpi in the presence of autophagy inducer AZD = AZD8055 and AZD/ConA. Puncta were calculated from z-stacks of n=10 individuals using ImageJ. Statistical significance (*** $P < 0.5$) was revealed by Student's t-test comparing

558 number of autophagosomes in AZD/ConA treatments in pTRV2 and pTRV2-*SH3P2* plants.
559 The experiment was repeated twice with similar results.
560 **(C)** Transient expression of GFP-ATG8E in pTRV2 and pTRV2-*SH3P2* plants with indicated
561 treatments (mock, AZD8055, AZD8055/ConA). Confocal images were taken at 1dpi. Scale
562 bars are indicated in the figure. Square indicates area that was used for a close-up image (Bar
563 = 5 µm).
564 **(D)** Growth of Xcv *and* Xcv *ΔxopL* strains in *roq1 N. benthamiana* plants silenced for SH3P2
565 and Joka2 (pTRV2-*SH3P2*, pTRV2-*Joka2*) compared to control plants (pTRV2). Leaves were
566 dip-inoculated with a bacteria suspension at OD_{600} = 0.2 and bacteria were quantified at 3, 6
567 dpi. Data represent the mean SD (n = 6) and n = 5 for pTRV2-*SH3P2*. Significant differences
568 were calculated using Student's *t-test* and are indicated by: *, P < 0.05; **, P < 0.01; ***, P <
569 0.001 The experiment was repeated more than more than two times with similar trends.
570

571 # Discussion

572

573 The role of autophagy in host-microbe interactions has remained enigmatic and puzzling.
574 Previous studies have reported that autophagy is modulated during host-bacteria interactions
575 and that bacterial effectors actively regulate this process (22, 55). Across kingdoms, autophagy
576 has both pro- and anti-bacterial activities (12, 25). In animals and also plant-virus interactions,
577 the role of anti-microbial autophagy has been attributed mostly to xenophagy, the autophagic
578 degradation of pathogens or pathogenic molecules which can be counteracted by microbial
579 effectors (13, 56). In contrast to animal pathogenic bacteria, plant gram negative pathogenic
580 bacteria reside in the apoplast without being in contact with the intracellular autophagy
581 machinery. The only bacterial components present inside the cell are T3Es that have been
582 shown to actively modulate autophagy responses (18, 26). However, little is known about how
583 they mechanistically regulate autophagy and whether they are potential targets of xenophagy.
584 Here, by studying *Xanthomonas*-host interactions, we revealed a complex-layered regulatory
585 role of autophagy in plant immunity. We demonstrate that anti-bacterial autophagy is activated
586 during Xanthomonas infection by targeting the bacterial effector XopL and utilizing
587 NBR1/Joka2-triggered selective autophagy. However, XopL might act as a trap to access the
588 autophagy machinery and suppress it for its own benefit. Indeed, we here unveil that E3 ligase
589 XopL associates with and ubiquitinates the autophagy component SH3P2 to degrade it by the
590 proteasome. This in turn, dampens autophagy, hampering the delivery of cargos, including
591 XopL, into the lytic vacuole. Both the block of autophagy and also rescue of XopL is beneficial
592 for the bacterium as anti-bacterial autophagy is eliminated and pathogenicity restored (Fig.
593 S16).
594 *Autophagy in host-immune interactions*
595 Over the recent years, autophagy has emerged as one of the main targets of animal and plant
596 pathogens, not only due to its role in maintaining a functional environment but also due to its
597 participation in immune responses (9, 57). In animals, several pathogenic bacteria have been
598 identified to modulate the autophagy pathway to their own benefit (12). Many intracellular
599 animal pathogenic bacteria can be eliminated by autophagy, while others (such as *Shigella*,
600 *Yersinia* and *Listeria*), are able to exploit autophagy to increase their pathogenicity (12). In
601 plants, several studies have highlighted that pathogens manipulate the autophagy pathway (58).
602 More specifically, the plant pathogenic bacterium *Pseudomonas syringae* pv. *tomato* (*Pst*) has
603 been shown to utilize effectors to modulate autophagic degradation (18, 26). However,
604 autophagy seems to display contrasting pro-and antibacterial effects. On the one hand,
605 autophagy is beneficial for the virulence of *Pst* while on the other hand, NBR1-dependent
606 autophagy restricts pathogen growth (18). With *Xcv,* we have identified another plant
607 pathogenic bacterium that modulates autophagy, similar to *Pst*, in an effector-dependent
608 manner. Although, both pathogens have the same habitat and hemi-biotrophic lifestyle, they act

609 in different ways on the autophagy pathway. For *Xcv* inhibition of the autophagy pathway is
610 crucial to maintain pathogenicity while *Pst* activates it for its own benefit. Previously, it has
611 been reasoned that autophagy activation might be essential to maintain plant viability and
612 lifespan (19). However, autophagy may not be required for this during *Xcv* infection, as it has
613 been shown that T3Es XopD and XopJ are able to prolong the biotrophic phase by other
614 mechanisms (38, 59). As such, autophagy is dispensable for the virulence of *Xcv* and actively
615 blocked to prevent xenophagy of effector(s). Within the realm of xenophagy, the degradation
616 of effectors by autophagy can be considered as a form of "effectorphagy". In turn, *Xanthomonas*
617 is able to block this process by targeting SH3P2 for degradation. SH3P2 was first identified as
618 a novel autophagy component, stimulating autophagosome formation during nitrogen
619 starvation and BTH-triggered immune responses (51). Later studies also showed that SH3P2
620 plays a key role in membrane tubulation during cell plate formation (60) and clathrin-mediated
621 endosomal sorting and degradation, with no effect in dark-induced autophagy (53). Our findings
622 that loss of SH3P2 from *N. benthamiana* impairs autophagy and promotes pathogenicity sheds
623 further light on its diverse functions. However, the effects of XopL on SH3P2 and increasing
624 virulence of *Xcv* might not only be attributed to its function in autophagy. Because endocytic
625 trafficking also plays a major role in plant immunity (61), it is likely that XopL has a function
626 beyond autophagy to impair plant defense mechanisms. This is also supported by the fact that
627 XopL is able to reduce PTI responses (41), which is not due its function in autophagy, as
628 autophagy deficiency has no impact on PTI responses (62). Previously, XopL was shown to
629 impact stromule formation by localizing to microtubules (54), which was shown only for the
630 XopL version lacking E3 ligase activity. Although, we do not see any microtubule localization
631 of the XopL ΔE3 version, XopL might affect stromule formation as they are thought to be
632 recognized by autophagic membranes prior autophagic degradation (2).
633 In summary, the anti- and pro-bacterial effects of autophagy seem to be very complex. In some
634 cases, both, anti- and pro-bacterial effects seem to operate during host-bacteria interactions.
635 Specifically, recent findings indicate that *Pst* seems to possess T3Es that are able to impair
636 autophagy (26). This suggests that multiple autophagy pathways with opposing effects might
637 operate in parallel. This apparent contradiction is supported by findings of animal pathogenic
638 bacteria: *Salmonella* has been shown to be degraded by p62-mediated selective autophagy but
639 at the very same time requires the autophagy pathway to replicate in HeLa cells (63, 64). These
640 findings add a certain complexity to the role of autophagy in host-microbe interactions that
641 might be explained by cell-type specific responses or operation of various selective autophagy
642 pathways that might be specifically targeted by the pathogens.
643 *Role of xenophagy in immunity*
644 One of the best studied selective autophagy receptors across kingdoms is NBR1/p62 that plays
645 a central role in xenophagy and degradation of protein aggregates (35, 67). Its role in plant
646 immune responses has been shown by the involvement of NBR/Joka2-mediated selective
647 autophagy in restricting pathogen growth or disease progression during *P. infestans* or *Pst*
648 infection (16, 18). In animals, p62, the counterpart of plant NBR1, functions to mediate
649 xenophagy, which has been also described for NBR1 in plants in a plant-virus infection context
650 but not for other plant pathogens (19, 20). Our analysis provides the first evidence that similar
651 to viral proteins, bacterial effectors may also constitute a target of NBR1-mediated selective
652 autophagy. We found that XopL is targeted by NBR1/Joka2 for autophagic degradation
653 shedding light on the function of NBR1/Joka2 to restrict pathogen growth. We hypothesize that
654 XopL might have been used as a bait to access the autophagy pathway in order to boost
655 virulence of *Xcv* by attenuating autophagic degradation. Initially, targeted by NBR1/Joka2-
656 dependent autophagy, a sub-proportion of XopL is "sacrificed" and ends up in the vacuole for
657 degradation. However, as XopL is able to associate with and degrade the autophagy component
658 SH3P2, it partially escapes its own degradation and blocks autophagy. Although, XopL is able
659 to suppress autophagy, its activity to block the pathway is still less than the recently discovered

660 AIMp, which acts as a potent autophagy inhibitor (34). This also explains why XopL is still
661 degraded. To date, it has not been reported that bacterial effectors in animals and plants are
662 removed by selective autophagy as an anti-microbial response. Although, a recent study by
663 Pandey et al. 2020 identified that an oomycete effector from *P. infestans* is degraded by
664 autophagy, its mode of action and consequences remain unknown (34). Interestingly, the
665 *Salmonella* effector SseL, which inhibits selective autophagy to abolish p62-dependent
666 degradation of *Salmonella*, was also found to interact with p62 (68). This might suggest the
667 possibility that SseL might also have been an autophagy target before it acquired its function to
668 block this pathway via its deubiquitinase activity (68). We hypothesize that NBR1/p62 might
669 have evolved to have a function in anti-bacterial autophagy by triggering xenophagy of bacterial
670 molecules as an alternative strategy to degrade entire intracellular bacteria. This may have
671 happened for the function of NBR1 in plants, as fungal and oomycete pathogens as well as gram
672 negative bacteria reside in the extracellular space. Animal pathogens also occupy the
673 extracellular space, before entering the host cell. In the case of *Salmonella*, it first needs to
674 inject bacterial effectors via its SPI-1 T3SS to establish internalization and its replication niche
675 (69). It is therefore tempting to speculate that these effectors may be targeted by selective
676 autophagy mechanisms as an early defense mechanism of the immune system. Similar to XopL,
677 several of the SPI1 T3Es, e.g., SopA as well as SopE can mimic E3 ligases and/or are
678 ubiquitinated in the host cell (70), making them ideal targets for NBR1/p62-mediated selective
679 autophagy. Indeed, SopA and SopE have been reported to be degraded through the proteasome
680 (71, 72). A possible degradation by autophagy was not investigated in these studies. Our results
681 also suggest that XopL is targeted by a host E3 ligase for degradation as the XopL variant
682 lacking E3 ligase activity is still ubiquitinated *in planta* and degraded by autophagy. Several
683 E3 ligases have been implicated in plant-microbe interactions, which opens up the possibility
684 that they may target microbial proteins (73).
685 Although plant pathogenic bacteria possess T3Es that are implicated in the host ubiquitin
686 system, to date there is no evidence that they might be ubiquitinated in the host. In addition, we
687 identified that XopL undergoes self-ubiquitination, which has not been reported for animal and
688 plant pathogenic bacterial effectors. This might constitute a novel mechanism how these
689 effectors exploit degradation system. To date, autoubiquitination of E3 ligases has been
690 assigned as a mechanism of self-regulation through which their activity is controlled (54). In
691 the case of bacterial T3Es that mimic E3 ligases, it might be a strategy to trick degradation
692 systems. Given the fact that XopL belongs to the IpaH E3 ligase family of effectors that are
693 widely conserved among animal and plant pathogens (74), we envision that similar mechanisms
694 might act across kingdoms. Indeed, T3E IpaH1.4 from *Shigella* blocks autophagy through a
695 different mechanism (75). Future research on the IpaH E3 ligase family of effectors might
696 reveal whether they possess self-ubiquitination activity and utilize this to trick the host immune
697 system or to modulate their activity within the host.
698 Taken together, we provide a primary example of an effector with self-ubiquitination activity
699 which makes it a target of selective autophagy. We provide evidence that by self-ubiquitination,
700 XopL first presents itself as a target of autophagy and then degrades the autophagy component
701 SH3P2, in order to block the autophagy machinery. Together, our observations uncover a novel
702 mechanism how a bacterial effector modifies itself to hijack the host autophagy system.
703
704
705
706
707
708
709

710 # Material and Methods
711
712 **Plant Material and Growth Conditions**
713 Wild-type plants were *Arabidopsis thaliana* ecotype Columbia (Col-0) and *Nicotiana*
714 *benthamiana. Arabidopsis* plants were grown on soil under short-day conditions (8/16-h
715 light/dark cycles) in a growth chamber or for maintenance and crossings under long-day
716 conditions (16/8-h light/ dark cycles) in a growth room with light intensity of 150 µE, 21°C,
717 and 70% relative humidity, respectively. *N. benthamiana* plants were grown under long day
718 conditions 16/8-h light/dark cycles, 21°C, and 70% relative humidity.
719
720 **Bacterial growth conditions**
721 *Agrobacterium tumefaciens*, Agrobacteria strain C58C1 was grown in LB Hi-Salt (10g/L
722 sodium chloride, 10g/L tryptone, 5g/L yeast extract) with 100 µg mL−1 rifampicin at 28 °C.
723 The cultures supplemented with the appropriate antibiotics for those harbouring plasmids. Xcv
724 strain 85-10 was grown in NYG media (0.5% peptone, 0.3% yeast extract, 2% glycerol) with
725 100 µg mL−1 rifampicin at 28 °C.
726
727 **Construction of Xcv Δ*xopL* and Δ*xopQ* null mutants**
728 To construct Xcv 85-10 *xopL* and *xopQ* deletion mutants, the 1.7-kb upstream and downstream
729 regions of the xopL or xopQ gene were PCR amplified using Xcv 85-10 genomic DNA as
730 template and cloned into pLVC18 linearized with EcoRI (New England Biolabs) using Gibson
731 assembly. The plasmid was introduced into Xcv 85-10 by triparental mating. Xcv
732 transconjugants were analysed by PCR to confirm that homologous recombination occurred at
733 the xopL or XopQ locus.
734
735 **Constructs for Xcv Δ*xopL* complementation analysis**
736 To construct xopL gene with 0.3-kb promoter region in broad host range vector, 0.3-kb
737 promoter-xopL gene was PCR amplified using Xcv 85-10 genomic DNA as template and
738 cloned into pBBR1MCS-2 (76) linearized with EcoRV (New England Biolabs) using Gibson
739 assembly. The plasmid was introduced into Xcv 85-10 Δ*xopL* by triparental mating.
740
741 **Bacterial infection**
742 Xcv carrying a deletion mutation of XopQ (Xcv *ΔxopQ*), or of HrcN (Xcv Δ*hrcN*), or of both
743 XopQ and XopL (Xcv *ΔxopQ ΔxopL*) were used to infect wild-type *N. benthamiana*. Xcv were
744 grown overnight in NYG with appropriate antibiotics at 28°C with shaking. Bacteria were
745 diluted to OD_{600} = 0.2 for dual-luciferase assays, immunoblot analysis of NBR1, ATG8 or
746 confocal microscopy of autophagosomal structures. For in planta growth curves using syringe
747 infiltration, Xcv strains were inoculated at OD_{600} = 0.0004, and for dip-inoculation OD_{600} = 0.2
748 was used.
749
750 **Tomato growth condition and bacterial growth assay**
751 Tomato (*Solanum lycopersicum*) cv. VF36 was grown in greenhouse (22-28 °C, 50-70 % RH,
752 16-h light). For bacterial growth assays, leaflets were dipped in a 2 x 10^8 CFU/mL suspension
753 of Xcv 85-10 strains in 10mM MgCl2 with 0.025% (v/v) silwet L-77 (Helena Chemical
754 Company) for 30 sec. Plants were then placed in plastic chambers at high humidity (>95%) for
755 24 h. For each strain analyzed, four leaf discs (0.5 cm^2) per treatment per timepoint were ground
756 in 10 mM $MgCl_2$ and diluted and spotted onto NYGA plates in triplicate to determine bacterial
757 load. Three biological replicates (i.e., three plants) were used, and the experiment was repeated
758 at least three times.
759
760

761 **Plasmid construction**
762 For transient expression experiments, the coding region of XopL, AtSH3P2 or SlJoka2 were
763 cloned into pENTR/D-TOPO and subsequently recombined into pUBN-DEST-GFP or RFP
764 (77), pGWB614/5 (78), pMAlc2, pDEST15. The RFP-ATG8E/G, GFP-ATG8e, RFP-NBR1,
765 RLUC-ATG8, RLUC-NBR1, XopD-GFP, XopJ-GFP, pTRV2-Joka2, pTRV2-ATG7
766 constructs were described previously (18, 38). All binary plasmids were transformed into
767 Agrobacterium tumefaciens strain C58C1 and infiltration of *N. benthamiana* was done at the
768 four-to six-leaf stage. Stable Arabidopsis transformation was performed using the floral dip
769 method (79).
770
771 **Transient Expression in *N. benthamiana* by Agrobacterium-Mediated Leaf Infiltration**
772 Agrobacterium strains harboring the indicated plasmids were grown overnight in liquid LB
773 media at 28°C with appropriate antibiotics and harvested by centrifugation at 4000g for 15 min.
774 Bacterial pellets were washed once in double-distilled water, resuspended in infiltration buffer
775 (10 mM MES, pH5.7, 10 mM $MgCl_2$, and 150 µM acetosyringone). The OD_{600} = 0.2 of each
776 culture was adjusted such that approximately equal numbers of bacteria from cultures
777 expressing different transgenes were mixed and infiltrated into *N. benthamiana* leaves using a
778 needleless syringe.
779
780 **Confocal Microscopy**
781 Live-cell images were acquired from abaxial leaf epidermal cells using a Zeiss LSM780 and
782 LSM880 microscope. Excitation/emission parameters for GFP and RFP were 488 nm/490 to
783 552 nm and 561 nm/569 to 652 nm, respectively, and sequential scanning mode was used for
784 colocalization of both fluorophores. Confocal images with ImageJ (version 2.00) software.
785 Quantification of ATG8a-labeled autophagosomal structures was done on z-stacks that were
786 converted to eight-bit grayscale and then counted for ATG8 puncta either manually or by the
787 Particle Analyzer function of ImageJ.
788
789 **FRET-FLIM measurement**
790 FRET-FLIM was performed on SP8 confocal laser scanning microscope (CLSM) (Leica
791 Microsystems GMBH) with LAS AF and SymPhoTime 64 software using a 63x/1.20 water
792 immersion objective. FLIM measurements were performed with a 470 nm pulsed laser (LDH-
793 P-C-470) with 40 MHz repetition rate and a reduced speed yielding, with an image resolution
794 of 256x256, a pixel dwell time of ~10 µs. Max count rate was set to ~15000 cps. Measurements
795 were stopped, when the brightest pixel had a photon count of 1000. The corresponding emission
796 was detected with a Leica HyD SMD detector from 500 nm to 530 nm by time-correlated single-
797 photon counting using a Timeharp260 module (PicoQuant, Berlin). The calculation of GFP
798 lifetime was performed by iterative reconvolution, i.e. the instrument response function was
799 convolved with exponential test functions to minimize the error with regard to the original
800 TCSPC histograms in an iterative process. For measurements of GFP-JOKA2 protein
801 aggregates, ROIs where drawn manually on SymphoTime64 software around the aggregates to
802 analyze GFP lifetime in these structures.
803
804 **Immunoprecipitation**
805 GFP pull-down assays were performed as previously described (18) with minor modifications.
806 Approximately 2 g of leaf material was ground to a fine powder in liquid nitrogen and
807 homogenized in 4 mL of extraction buffer (25 mM Tris-HCl, pH 7.5, 150 mM NaCl,
808 10%glycerol, 1 mM DTT, 1 mM EDTA, 1% [v/v] protease inhibitor cocktail, and 0.5%
809 TritonX). Insoluble debris was pelleted by centrifugation for 20 min with 4000 rpm at 4°C.
810 Immunoprecipitation was performed by adding 30 mL of GFP-Trap coupled to agarose beads
811 (ChromoTek) and samples were incubated for 2 h at 4°C with continual rotation. Beads were

812 subsequently washed five times with Tris-buffered saline containing 0.5% Triton X, and
813 immunoprecipitates were eluted with 30 µL of 2x SDS loading buffer at 70°C for 10 min.
814 Pulldown of ubiquitinated proteins according to manufacturer's instructions (NanoTag
815 Biotechnologies).
816
817 ***In vitro* pull-down**
818 Recombinant proteins from *Escherichia coli* lysates were immobilized on amylose resins (New
819 England Biolabs), incubated for 1 h at 4 °C with purified GST-SH3P2, eluted, and analyzed by
820 immunoblotting using either anti-GST antibody (Sigma) or anti- MBP antibody (NEB).
821
822 ***In vitro* ubiquitination assay**
823 Recombinant proteins were expressed in *E. coli* BL21(DE3) and purified by affinity
824 chromatography using amylose resin (New England Biolabs). Recombinant His-UBA1 and
825 His-UBC8 were purified using Ni-Ted resin (Macherey-Nagel). Purified proteins were used for
826 *in vitro* ubiquitination assays. Each reaction of 30 mL final volume contained 25 mM Tris-HCl,
827 pH 7.5, 5 mM MgCl2, 50 mM KCl, 2 mM ATP, 0.6 mM DTT, 2 µg ubiquitin, 200 ng E1 His-
828 *At*UBA1, 1.2 µg E2 His-*At*UBC8, 2 µg of E3s, and 0.3 µg of MBP-*At*SH3P2. Samples were
829 incubated for 1h at 30°C and reaction was stopped by adding SDS loading buffer and incubated
830 for 10 min at 68°C. Samples were separated by SDS-PAGE electrophoresis using 4–15% Mini-
831 PROTEAN® TGX™ Precast Protein Gels (BioRad) followed by detection of ubiquitinated
832 substrate by immunoblotting using anti-MBP (New England Biolabs), anti-GST and anti-
833 ubiquitin (Santa Cruz Biotechnology) antibodies.
834
835 **Immunoblot analysis**
836 Proteins were extracted in 100 mM Tris (pH 7.5) containing 2% SDS, boiled for 10min in SDS
837 loading buffer, and cleared by centrifugation. The protein extracts were then separated by SDS-
838 PAGE, transferred to PVDF membranes (Biorad), blocked with5% skimmed milk in PBS, and
839 incubated with primary antibodies anti-NBR1 (Agrisera), anti-ATG8 (Agrisera), anti-ubiquitin
840 (Agrisera), anti-GFP (SantaCruz), anti-RFP (Chromotek), anti-HA (Sigma Aldrich) primary
841 antibodies using 1:2000 dilutions in PBS containing 0.1% Tween 20. This was followed by
842 incubation with horseradish peroxidase-conjugated secondary antibodies diluted 1:10,000 in
843 PBS containing 0.1% Tween 20. The immunoreaction was developed using an ECL Prime Kit
844 (GE Healthcare) and detected with Amersham Imager 680 blot and gel imager.
845
846 **Dual Luciferase Assay**
847 The dual luciferase reporter assay was performed according to the manufacturer's instructions
848 (Dual-Luciferase Reporter Assay System; Promega) with slight modifications. Briefly, four leaf
849 discs were homogenized in 200 µL lysis buffer and cleared by centrifugation. For detection and
850 measurement of the Fireflyluciferaseactivity,40 µL of the luciferase assay reagent was added to
851 5 µL of plant extracts. To measure *Renilla* luciferase activity, 40 µL of the Stop and Glo reagent
852 was added to the mixture. The measurement was performed in a plate reader.
853
854 **Virus-induced gene silencing**
855 VIGS was performed as described previously (38). In brief, fragment of SH3P2 was amplified
856 by PCR and cloned into pTRV2-Gateway using the Gateway recombination system. Primer
857 sequences are listed in Supplemental Table 1 online. The resulting plasmids were transformed
858 into *Agrobacterium tumefaciens* C58C1. A lower leaf of a 2-week-old *N. benthamiana* plant
859 (four-leaf stage) was co-infiltrated with a mixture of Agrobacteria carrying either pTRV1, a
860 binary vector expressing TRV subgenomic RNA1 under control of the cauliflower mosaic virus
861 35S promoter, or pTRV2 expressing TRV subgenomic RNA2 and containing the target
862 sequence. Silenced plants were analyzed 14 d after infiltration.

863
864 **RNA extraction and RT-qPCR**
865 RNA was extracted from 4 leaf discs according to manufacturer instructions using the
866 GeneMATRIX Universal RNA Purification Kit (Roboklon) with on-column DNase I digestion.
867 RNA integrity was checked by loading on 1% agarose gel and separating by electrophoresis.
868 RNA concentrations were measured using Nanodrop 2000 (Thermo Fisher), and equal amounts
869 of RNA were used for cDNA synthesis. cDNA synthesis was performed using LunaScript™
870 RT SuperMix Kit (New England Biolabs) and in a standard thermocycler according to
871 manufacturer instructions. Gene expression was measured by qPCR using MESA BLUE qPCR
872 MasterMix Plus for SYBR® Assay No ROX (Eurogentec) and cycle quantification by Biorad
873 CFX system.
874
875 **NanoLC-MS/MS analysis and data processing**
876 Proteins were purified on an NuPAGE 12% gel (Invitrogen) and Coomassie-stained gel pieces
877 were digested in gel with trypsin as described previously (80) with a small modification:
878 chloroacetamide was used instead of iodoacetamide for carbamidomethylation of cysteine
879 residues to prevent formation of lysine modifications isobaric to two glycine residues left on
880 ubiquitinylated lysine after tryptic digestion. After desalting using C18 Stage tips peptide
881 mixtures were run on an Easy-nLC 1200 system coupled to a Q Exactive HF-X mass
882 spectrometer (both Thermo Fisher Scientific) as described elsewhere (81) with slight
883 modifications: the peptide mixtures were separated using a 87 minute segmented gradient from
884 10-33-50-90% of HPLC solvent B (80% acetonitrile in 0.1% formic acid) in HPLC solvent A
885 (0.1% formic acid) at a flow rate of 200 nl/min. The seven most intense precursor ions were
886 sequentially fragmented in each scan cycle using higher energy collisional dissociation (HCD)
887 fragmentation. In all measurements, sequenced precursor masses were excluded from further
888 selection for 30 s. The target values were 105 charges for MS/MS fragmentation and 3x106
889 charges for the MS scan.
890 Acquired MS spectra were processed with MaxQuant software package version 1.5.2.8 with
891 integrated Andromeda search engine. Database search was performed against a *Nicotiana*
892 *benthamiana* database containing 74,802 protein entries, the sequences of XopL from
893 *Xanthomonas campestris* pv. *vesicatoria*, and 285 commonly observed contaminants.
894 Endoprotease trypsin was defined as protease with a maximum of two missed cleavages.
895 Oxidation of methionine, phosphorylation of serine, threonine and tyrosine, GlyGly dipetide on
896 lysine residues, and N-terminal acetylation were specified as variable modifications.
897 Carbamidomethylation on cysteine was set as fixed modification. Initial maximum allowed
898 mass tolerance was set to 4.5 parts per million (ppm) for precursor ions and 20 ppm for fragment
899 ions. Peptide, protein and modification site identifications were reported at a false discovery
900 rate (FDR) of 0.01, estimated by the target-decoy approach (Elias and Gygi). The iBAQ
901 (Intensity Based Absolute Quantification) and LFQ (Label-Free Quantification) algorithms
902 were enabled, as was the "match between runs" option (82).
903
904 **Drug treatments**
905 For the analysis of protein stability 200 mM MG132 or 1% EtOH was infiltrated to plants
906 transiently expressing binary constructs 2dpi. 6 hours later leaf material was harvested. were
907 analysed under the CLSM. Concanamycin A treatment was performed by syringe infiltration
908 of mature leaves with 0.5 µM ConA for 6-8 h prior confocal analysis or immunoblot analysis.
909 AZD8055 (15 µM) was done for 6-8 hours prior confocal microscopy.
910
911 **Phylogenetic Analysis**
912 An alignment between SH3P2 proteins was generated using ClustalW wand the tree was
913 generated using the neighbor-joining method.

Data Analysis and Presentation

Data are presented as mean SD. Statistical significance was analysed by Student's t test (*P < 0.05, **P < 0.01, and P*** < 0.001). The number of biological replicates (n) is given in the figure legends. Statistical analyses and graphical presentation of data were made in R and RStudio (Version 1.2.5033). Boxplots were prepared using the ggplot2 package.

Supporting information

Figure S1: Virus-induced gene silencing of *ATG7* in *N. benthamiana* plants.
Figure S2: Suppression of autophagy is enhanced by T3Es**.**
Figure S3: Screening for Xanthomonas T3Es with altered autophagic flux.
Figure S4: XopL is an essential virulence factor
Figure S5: Transgenic *A. thaliana* GFP-XopL plants display defects in autophagic degradation.
Figure S6: XopL is degraded in the vacuole.
Figure S7: Confirmation of efficient silencing of NBR1/Joka2.
Figure S8: XopL is ubiquitinated *in planta*.
Figure S9: XopL undergoes self-ubiquitination.
Figure S10: Localization of GFP-XopL$_{K191A}$ in *N. benthamiana*.
Figure S11: GFP-XopL$_{K191A}$ is still ubiquitinated in planta.
Figure S12: SH3P2 is conserved in different plant species.
Supplemental Video 1: XopL/SH3P2 puncta are mobile.
Figure S13: RFP-XopL ΔE3 co-localizes with SH3P2-GFP.
Figure S14: Protein levels of GFP-XopL ΔE3 are stabilized by AIMp and ConA treatment.
Figure S15: Virus-induced gene silencing of SH3P2 in *N. benthamiana* plants.
Figure S16: Model illustrating the function of XopL.
Supplemental Table 1: Primers used in manuscript.

Author contributions

J.-X.L, S.Ü., M.R., D.S., G.L., A.R.G., J.-G.K., M.F.-W. performed the experiments. E.A.M., M.F.W., B.M., A.H., T.O.B., M.B.M., F.B., D.H., and S.Ü. analysed the data. P.P. and T.O.B. provided unpublished material. S.Ü. planned the project and wrote the article with input from all authors.

Acknowledgements

We thank Ingrid Schießl for the initial Y2H screen with XopL. We also thank Tom Denyer for critical reading of the manuscript. We thank Johannes Stuttmann for the *roq1 N. benthamiana* seeds. We thank Silke Wahl and Irina Droste-Borel for technical support for the proteomics assay. This work was supported by an Emmy Noether Fellowship GZ: UE188/2-1 from the Deutsche Forschungsgemeinschaft (DFG; to S.Ü.), and through the collaborative research council 1101 (SFB1101; to G.L.). E.A.M. was supported by EU Horizon 2020 MSCA IF (799433). F.B. was supported by funds from the DFG (BO1961/5-2). D.H. was supported by grants from the Swedish research councils VR (2016-04562; 2020-05327) and FORMAS (2017-01596). T.O.B. was supported by BBSRC - Biotechnology and Biological Sciences Research Council, grant code BB/T006102/1. M.B.M. was supported by NSF IOS Grant 2026368. FORMAS (grant number 2016-01044) for A.H.

964 # Figure Legends
965
966 **Figure 1: Xanthomonas blocks autophagy to enhance its pathogenicity**
967 **(A)** Autophagic flux determined by quantitative dual-luciferase assay. RLUC-ATG8a or
968 RLUC-NBR1 constructs were coexpressed with internal control FLUC in *N. benthamiana*. *Xcv*
969 *ΔxopQ* was co-infiltrated with Agrobacteria containing the Luciferase constructs. Coexpression
970 of RFP-AIMp serves as a control for autophagy inhibition. Expression of the latter was
971 confirmend with western blot (inset). Renilla (RLUC) and Firefly (FLUC) luciferase activities
972 were simultaneously measured in leaf extracts at 48 h post- infiltration using the dual-luciferase
973 system. Values represent the mean ratio of RLUC-ATG8a and FLUC activities and error bars
974 show SD (n=4). Statistical significance (***P<0.001) was revealed by Student's *t*-test. The
975 experiment was repeated more than 3 times with similar results.
976 **(B)** RFP-ATG8g-labeled autophagosomes were quantified from plants infected with mock or
977 Xcv *ΔxopQ* at 2 dpi in the presence or absence of ConA (bars = 20 µm). Puncta were calculated
978 Puncta were calculated from z-stacks (15) of n=6 individuals using ImageJ. Center lines show
979 the medians; box limits indicate the 25th and 75th percentiles as determined by R software;
980 whiskers extend 1.5 times the interquartile range from the 25th and 75th percentiles and data
981 points are plotted as open circles. Different letters indicate statistically significant differences
982 (P < 0.05) as determined by one way ANOVA. The experiment was repeated twice with similar
983 results.
984 **(C)** Immunoblot analysis of NBR1 and ATG8 protein levels in Xcv *ΔxopQ* or mock infected
985 *N. benthamiana* plants at 1 and 2dpi. Agrobacterium-mediated transient expression of RFP-
986 AIMp serves as a control for autophagy suppression. Ponceau Staining (PS) served as a loading
987 control. The experiment was repeated three times with similar results.
988 **(D)** RT-qPCR analysis of *NbATG8-1.1/2, NbATG8-2.1/2* and *NbJoka2* transcript levels upon
989 challenge of *N. benthamiana* plants with Xcv *ΔxopQ* for 1 and 2 dpi compared to mock infected
990 plants. Values represent mean + SD (n=4) relative to mock control of respective time point and
991 were normalized to *PP2A*. Statistical significance (*P < 0.05, **P < 0.01, *** P < 0.001) was
992 revealed by Student's *t*-test.
993 **(E)** Bacterial density in leaves of *N. benthamiana* infected with Xcv *ΔxopQ* in the presence or
994 absence autophagy suppressor RFP-AIMp. Leaves were syringe infiltrated with OD_{600} =
995 0.0004, and colony-forming units were counted at 6 dpi. Compared to empty vector control
996 (EV), AIMp expressing plants (n=6) harbour significantly more bacteria. Statistical
997 significance (*P < 0.05) was revealed by Student's *t*-test. Expression of RFP-AIMp was
998 verified at 6 dpi with an anti-RFP blot (n=4).
999
1000 **Figure 2: Xanthomonas T3E XopL is suppressing autophagy**
1001 **(A)** RLUC-ATG8a or RLUC-NBR1 constructs were coexpressed with internal control FLUC
1002 in *N. benthamiana*. XopL or control (Ctl) constructs were co-infiltrated. RLUC and FLUC
1003 activities were simultaneously measured in leaf extracts at 48 h post- infiltration using the dual-
1004 luciferase system. Values represent the mean ratio of RLUC-ATG8a and FLUC activities and
1005 error bars show SD (n=4). Statistical significance (* P < 0.5, ** P < 0.01) was revealed by
1006 Student's *t*-test. The experiment was repeated more than 3 times by 2 different people with
1007 similar results.
1008 **(B)** Immunoblot analysis of NBR1 and ATG8 protein levels in *N. benthamiana* plants
1009 transiently expressing GFP-XopL or GFP control at 2dpi. Expression of GFP-XopL and GFP
1010 were verified with an anti-GFP antibody. Ponceau Staining (PS) served as a loading control. T
1011 The experiment was repeated at least three times by 2 different people with similar results.
1012 **(C)** Immunoblot analysis of NBR1 and ATG8 protein levels in *N. benthamiana* plants
1013 transiently expressing XopL or GUS control at 2dpi in the presence or absence of ConA.
1014 Expression of GFP-XopL was verified with an anti-GFP antibody, while expression of GUS-

1015 HA was confirmed with an anti-HA antibody. Ponceau Staining (PS) served as a loading
1016 control. The experiment was repeated twice with similar results.
1017 **(D)** RLUC-ATG8a or RLUC-NBR1 constructs were coexpressed with internal control FLUC
1018 in *N. benthamiana*. Xcv *ΔxopQ and* Xcv *ΔxopQ ΔxopL* were co-infiltrated with Agrobacteria
1019 containing the respective constructs. RLUC and FLUC activities were simultaneously measured
1020 in leaf extracts at 48 h post- infiltration using the dual-luciferase system. Values represent the
1021 mean ratio of RLUC-ATG8a and FLUC activities and error bars show SD (n=4). Statistical
1022 significance (***$P < 0.001$) was revealed by Student's *t*-test. The experiment was repeated 3
1023 times with similar results.
1024 **(E)** Immunoblot analysis of NBR1 and ATG8 protein levels in Xcv *ΔxopQ,* Xcv *ΔxopQ ΔxopL*
1025 or mock infected *N. benthamiana* plants at 2dpi. Ponceau Staining (PS) served as a loading
1026 control. The experiment was repeated twice with similar results.
1027
1028 **Figure 3: XopL is ubiquitinated in planta and degraded by NBR1-mediated selective**
1029 **autophagy**
1030 **(A)** Autophagy suppression enhances XopL stability. GFP-XopL was coexpressed with GFP or
1031 RFP-AIMp. Proteins were separated by SDS-PAGE and detected by immunoblotting using the
1032 indicated antibodies. Ponceau Staining (PS) served as a loading control. The experiment was
1033 repeated three times by two different people with similar results.
1034 **(B)** Colocalization of GFP-XopL with RFP-Joka2 in *N. benthamiana* leaves. Imaging was
1035 performed 2 d after transient expression and images represent single confocal planes from
1036 abaxial epidermal cells (bars = 20 µm). The experiment was repeated twice with similar results.
1037 **(C)** FRET FLIM measurements of GFP-Joka2 and RFP-XopL in *N. benthamiana* leaves. The
1038 freeRFP construct served as a negative control and RFP-ATG8E (n = 9) as a positive control.
1039 Scattered points show individual data points, color indicates biological repeats. The lifetime (in
1040 ns) of GFP-Joka2 (donor, n = 41) was significantly reduced in the presence of RFP-XopL (n =
1041 40) but not in the presence of freeRFP (n = 35). Significant differences were calculated using
1042 Wilcoxon rank sum test. The experiment was repeated three times with similar results.
1043 **(D)** Immunoprecipitation (IP) of GFP-XopL reveals association with NBR1. Immunoblots of
1044 input and IP samples from *N. benthamiana* plants transiently expressing GFP or GFP-XopL
1045 were probed with anti-GFP and anti-NBR1 antibodies.
1046 **(E)** Immunoprecipitation (IP) of GFP-XopL and GFP-XopL ΔE3 reveals association with
1047 NBR1. Immunoblots of input and IP samples from *N. benthamiana* plants transiently
1048 expressing GFP, GFP-XopL and GFP-XopL ΔE3 were probed with anti-GFP and anti-NBR1
1049 antibodies.
1050 **(F)** Stability of XopL is increased in Joka2 silenced plants. GFP-XopL was transiently
1051 expressed in pTRV2, pTRV2-Joka2 and *N. benthamiana* WT plants. Expression of binary
1052 constructs was verified with an anti-GFP antibody. Joka2 silencing was verified using an anti-
1053 NBR1 antibody. Ponceau Staining (PS) served as a loading control. The experiment was
1054 repeated twice with similar results.
1055 **(G)** Growth of Xcv *ΔxopQ* in *N. benthamiana* plants silenced for *Joka2* (pTRV2-Joka2)
1056 compared to control plants (pTRV2). Leaves were dip-inoculated with a bacteria suspension at
1057 $OD_{600} = 0.2$. and bacteria were quantified at 3 and 6 dpi. Data represent the mean SD (n = 6).
1058 Significant differences were calculated using Student's *t-test* and are indicated by: ***, P <
1059 0.001. The experiment was repeated three times with similar trends.
1060 **(H)** XopL is ubiquitinated *in planta*. GFP-XopL, GFP-XopL ΔE3 were transiently expressed
1061 in *N. benthamiana*. RFP-AIMp was co-infiltrated to stabilize both XopL variants. Samples were
1062 taken 48 hpi, and total proteins (Input) were subjected to immunoprecipitation (IP) with GFP-
1063 Trap beads, followed by immunoblot analysis of the precipitates using either anti-GFP or anti-
1064 ubiquitin antibodies. GFP served as a negative control. RFP-AIMp expression was verified by
1065 an anti-RFP antibody. The experiment was repeated three times with similar results.

1066 **(I)** XopL is ubiquitinated *in planta*. GFP-XopL was transiently expressed in *N. benthamiana*.
1067 RFP-AIMp was co-infiltrated to stabilize GFP-XopL. Samples were taken 48 hpi, and total
1068 proteins (Input) were subjected to immunoprecipitation (IP) with the ubiquitin pan selector,
1069 followed by immunoblot analysis of the precipitates using either anti-GFP or anti-ubiquitin
1070 antibodies. GFP served as a control. RFP-AIMp expression was verified by an anti-RFP
1071 antibody. Asterisk indicates the GFP-XopL full-length protein. The experiment was repeated
1072 three times with similar results.
1073 **(J)** Immunoblot analysis GFP-XopL and GFP-XopL$_{K191A}$ at 1 and 2 dpi using an anti-GFP
1074 antibody. Ponceau Staining (PS) served as a loading control. The experiment was repeated three
1075 times by two different people with similar results.
1076 **(K)** Mutation of Lysin 191 does not abolish poly-ubiquitination of XopL and association with
1077 NBR1. GFP-XopL and GFP-XopL$_{K191A}$ were transiently expressed in *N. benthamiana*. Samples
1078 were taken 48 hpi, and total proteins (Input) were subjected to immunoprecipitation (IP) with
1079 GFP-Trap beads, followed by immunoblot analysis of the precipitates using either anti-GFP,
1080 anti-ubiquitin and anti-NBR1 antibodies. GFP served as a control. The experiment was repeated
1081 three times with similar results.
1082
1083 **Figure 4: XopL interacts with SH3P2 and mediates its proteasome degradation via its E3**
1084 **ligase activity to block autophagy**
1085 **(A)** Interaction of XopL with SH3P2 in yeast two-hybrid assays. XopL fused to the GAL4
1086 DNA-binding domain was expressed in combination with SH3P2 fused to the GAL4 activation
1087 domain (AD) in yeast strain Y190. Cells were grown on selective media before a LacZ filter
1088 assay was performed. pSV40/p53 served as positive control, while the empty AD or BD vector
1089 served as negative control. NtSH3P2 = *Nicotiana tabacum* SH3P2. –LT = yeast growth on
1090 medium without Leu and Trp, –HLT = yeast growth on medium lacking His, Leu, and Trp,
1091 indicating expression of the HIS3 reporter gene. LacZ, activity of the lacZ reporter gene.
1092 **(B)** Coimmunoprecipitation of GFP-XopL with AtSH3P2-HA. GFP-XopL or GFP were
1093 transiently coexpressed with AtSH3P2-HA in leaves of *N. benthamiana*. After 48 h, total
1094 proteins (Input) were subjected to immunoprecipitation (IP) with GFP-Trap beads, followed by
1095 immunoblot analysis using either anti-GFP or anti-HA antibodies. AtSH3P2 = *Arabidopsis*
1096 *thaliana* SH3P2. Two repetitions with similar results have been conducted.
1097 **(C)** Visualization of protein interactions *in planta* by the bimolecular fluorescence
1098 complementation assay. Yellow fluorescent protein (YFP) confocal microscopy images show
1099 *Nicotiana benthamiana* leaf epidermal cells transiently expressing Venus^{N173}-XopL in
1100 combination with AtSH3P2-Venus^{C155}. A positive control showing the dimerization of
1101 fructose-1,6-bisphosphatase (FBPase) within the cytosol. The combination of Venus^{N173}-XopL
1102 with FBPase-Venus^{C155} or Venus^{N173}-FBPase with AtSH3P2-Venus^{C155} do not induce YFP
1103 fluorescenc and serve as negative controls. Bars = 20 µm. AtSH3P2 = *Arabidopsis thaliana*
1104 SH3P2. The experiment has been repeated twice with similar results.
1105 **(D)** *In vitro* co-IP assay showing direct interaction of XopL with AtSH3P2. MBP-XopL and
1106 GST-AtSH3P2 were expressed in E. coli. Pull down was performed using amylose resin.
1107 Proteins were detected in an immunoblot using antibodies as indicated.
1108 **(E)** Colocalization analysis of GFP-XopL with SH3P2-RFP, RFP-ATG8e and RFP-ATG8g in
1109 *N. benthamiana* leaves. Imaging was performed 2 d after transient expression and images
1110 represent single confocal planes from abaxial epidermal cells (scale bars = 20 µm and 10 µm,
1111 lower panel). The experiment was repeated twice with similar results.
1112 **(F)** Total proteins were extracted 48 hpi with *A. tumefaciens* harboring the respective GFP-
1113 XopL, HA-XopL and SH3P2-GFP expression constructs. SH3P2-GFP protein levels (lower
1114 band) were detected using an anti-GFP antibody. Expression of the XopL was verified using an
1115 anti-HA or anti-GFP antibody. Expression of GUS-HA served as a control. Ponceau S staining
1116 serves as a loading control. The experiment was repeated three times with similar results.

(G) SH3P2-GFP was transiently coexpressed together with GUS-HA and GFP-XopL in *N. benthamiana* using agroinfiltration. At 42 hpi, 200 mM MG132 was infiltrated into *A. tumefaciens*-inoculated leaves, and leaf material was collected 48 hpi. Expression of SH3P2-GFP (lower band) and GFP-XopL (upper band) was detected using an anti-GFP antibody. GUS-HA expression was confirmed with an anti-HA antibody. Ponceau S staining serves as a loading control. The experiment was repeated three times with similar results.
(H) *In vitro* ubiquitination assay reveals ubiquitination of SH3P2 by XopL. GST-XopL, and MBP-SH3P2 were tested using the Arabidopsis His-AtUBA1 and His-AtUBC8. Lanes 2 to 4 are negative controls. Proteins were separated by SDS-PAGE and detected by immunoblotting using the indicated antibodies. The experiment was repeated twice with similar results.
(I) SH3P2-GFP was transiently coexpressed together with GFP, GFP-XopL, GFP-XopL ΔE3 and RFP-XopL ΔE3 in *N. benthamiana* using agroinfiltration. GFP protein levels were detected with an anti-GFP antibody. Ponceau S staining serves as a loading control. The experiment was repeated three times with similar results.
(J) Immunoblot analysis of ATG8 protein levels in *N. benthamiana* plants transiently expressing GFP-XopL, GFP-XopL ΔE3 or GFP control at 2dpi. Expression of binary constructs was verified with an anti-GFP antibody. Ponceau Staining (PS) served as a loading control. The experiment was repeated twice with similar results.
(K) RLUC-ATG8a constructs were coexpressed with internal control FLUC in *N. benthamiana*. GFP-XopL, GFP-XopL ΔE3 or GFP control were co-infiltrated together with RLUC/FLUC mixture. *Renilla* and *Firefly* luciferase activities were simultaneously measured in leaf extracts at 48 hpi using the dual-luciferase system. Values represent the mean ratio of RLUC-ATG8a and FLUC activities and error bars show SD (n=4). Statistical significance (* $P < 0.5$, ** $P < 0.01$) was revealed by Student's *t*-test. The experiment was repeated 3 times by 2 different people with similar results. Expression of proteins was verified with indicated antibodies.

Figure 5: Silencing of SH3P2 suppresses autophagic degradation and is beneficial for *Xanthomonas* growth

(A) Immunoblot analysis of ATG8 protein levels in *N. benthamiana* pTRV2 (control) and pTRV2-*SH3P2* (*SH3P2* silencing) 2 weeks after VIGS. Ponceau Staining (PS) served as a loading control. The experiment was repeated twice with similar results.
(B) GFP-ATG8e-labeled autophagosomes were quantified from pTRV2 or pTRV2-SH3P2 plants transiently expressing GFP-ATG8e at 2dpi in the presence of autophagy inducer AZD = AZD8055 and AZD/ConA. Puncta were calculated from z-stacks of n=10 individuals using ImageJ. Statistical significance (*** $P < 0.5$) was revealed by Student's *t*-test comparing number of autophagosomes in AZD/ConA treatments in pTRV2 and pTRV2-*SH3P2* plants. The experiment was repeated twice with similar results.
(C) Transient expression of GFP-ATG8E in pTRV2 and pTRV2-*SH3P2* plants with indicated treatments (mock, AZD8055, AZD8055/ConA). Confocal images were taken at 1dpi. Scale bars are indicated in the figure. Square indicates area that was used for a close-up image (Bar = 5 μm).
(D) Growth of Xcv *and* Xcv *ΔxopL* strains in *roq1 N. benthamiana* plants silenced for SH3P2 and Joka2 (pTRV2-*SH3P2*, pTRV2-*Joka2*) compared to control plants (pTRV2). Leaves were dip-inoculated with a bacteria suspension at OD_{600} = 0.2 and bacteria were quantified at 3, 6 dpi. Data represent the mean SD (n = 6) and n = 5 for pTRV2-*SH3P2*. Significant differences were calculated using Student's *t-test* and are indicated by: *, $P < 0.05$; **, $P < 0.01$; ***, $P < 0.001$ The experiment was repeated more than more than two times with similar trends.

Fig. S1: Virus-induced gene silencing of *ATG7* in *N. benthamiana* plants.

1167 **(A)** Growth of Xcv *ΔxopQ* in *N. benthamiana* plants silenced for *ATG7* (pTRV2-*ATG7*)
1168 compared to control plants (pTRV2). Leaves were dip-inoculated with a bacteria suspension at
1169 OD_{600} = 0.2 and bacteria were quantified at 6 dpi. Data represent the mean SD (n = 6).
1170 Significant differences were calculated using Student's *t-test* and are indicated by *, P < 0.05.
1171 The experiment was repeated twice with similar trends.
1172 **(B)** qRT-PCR analysis of *ATG7* mRNA levels in silenced pepper plants. *Actin* expression was
1173 used to normalize the expression value in each sample, and relative expression values were
1174 determined against pTRV2 control plants, which was set to 1**.**
1175
1176 **Fig. S2: Suppression of autophagy is enhanced by T3Es.**
1177 **(A)** Autophagic flux determined by quantitative dual-luciferase assay. RLUC-ATG8a or
1178 RLUC-NBR1 constructs were coexpressed with internal control FLUC in *N. benthamiana*. Xcv
1179 *ΔxopQ* and *ΔhrcN* were co-infiltrated with Agrobacteria containing the respective constructs.
1180 Renilla and Firefly luciferase activities were simultaneously measured in leaf extracts at 48 h
1181 post- infiltration using the dual-luciferase system. Values represent the mean ratio of RLUC-
1182 ATG8a and FLUC activities and error bars show SD (n=4). Statistical significance (**P<0.01)
1183 was revealed by Student's *t*-test. The experiment was repeated 2 times with similar results.
1184 **(B)** Immunoblot analysis of NBR1 and ATG8 protein levels in Xcv *ΔxopQ, ΔhrcN* or mock
1185 infected *N. benthamiana* plants at 1 and 2dpi. Ponceau Staining (PS) served as a loading control.
1186 The experiment was repeated twice with similar results.
1187 **(C)** RT-qPCR analysis of *NbATG8-1.1/2, NbATG8-2.1/2* and *NbJoka2* transcript levels upon
1188 challenge of *N. benthamiana* plants with Xcv *ΔxopQ* and *ΔhrcN* for 1 and 2 dpi compared to
1189 mock infected plants. Values represent mean + SD (n=4) relative to mock control of respective
1190 time point and were normalized to *PP2A*. Statistical significance (**P < 0.01, *** P < 0.001)
1191 was revealed by Student's *t*-test.
1192
1193 **Fig. S3: Screening for Xanthomonas T3Es with altered autophagic flux.**
1194 **(A)** RLUC-ATG8a constructs were coexpressed with internal control FLUC in *N. benthamiana*.
1195 XopL, XopJ, XopD and XopS were co-infiltrated with the RLUC/FLUC mixture. Renilla and
1196 Firefly luciferase activities were simultaneously measured in leaf extracts at 48 h post-
1197 infiltration using the dual-luciferase system. Values represent the mean ratio of RLUC-ATG8a
1198 and FLUC activities and error bars show SD (XopL, XopJ, XopD, AIMp; n=20; XopS n=4).
1199 GFP served as a control and was set to 1. Expression of T3Es and RFP-AIMp were verified
1200 with the indicated antibodies. **(B)** RLUC-ATG8a constructs were coexpressed with internal
1201 control FLUC in *N. benthamiana*. Plants were treated with MG132 for 6 hours prior
1202 measurement. Values represent the mean ratio of RLUC-ATG8a and FLUC activities and error
1203 bars show SD (n=8). Statistical significance (* P < 0.5) was revealed by Student's *t*-test.
1204
1205 **Fig. S4: XopL is an essential virulence factor**
1206 **(A)** Growth of Xcv 85-10 (vector) (white bar), Xcv 85-10 Δ*xopL* (vector) (grey bar), and Xcv
1207 85-10 Δ*xopL* (*xopL*) (black bar) strains in tomato VF36 leaves. Leaves were dipped in a 2 x 10^8
1208 CFU/mL suspension of bacteria. The number of bacteria in each leaf was quantified at 10 dpi.
1209 Data points represent mean $\log_{10}$ colony-forming units per cm^2 ± SD of three plants. Different
1210 letters above bars indicate statistically significant (Tukey's honestly significant difference
1211 (HSD) test, P < 0.05) differences between samples. Vector = pBBR1MCS-2.
1212 **(B)** Delayed disease symptom development in tomato leaves inoculated with *Xcv* or *Xcv* Δ*xopL*.
1213 Tomato leaves inoculated with strains described in (A) were photographed at 14 dpi.
1214 **(C)** Growth of Xcv 85-10, Xcv 85-10 Δ*xopL* strains in *roq1 N. benthamiana* leaves. Leaves
1215 were dipped in a 2 x 10^8 CFU/mL suspension of bacteria. The number of bacteria in each leaf
1216 was quantified at 10 dpi. Data represent the mean SD (n = 5). Significant differences were

calculated using Student's *t-test* and are indicated by **, P < 0.01. The experiment was repeated twice with similar trends.
(D) Delayed disease symptom development in *roq1 N. benthamiana* leaves inoculated with *Xcv* or *Xcv* Δ*xopL*. *N. benthamiana roq1* leaves inoculated with strains described in (C) were photographed at 10 dpi.
(E) Delayed symptom development in *roq1 N. benthamiana* leaves inoculated with *Xcv* or *Xcv* Δ*xopL*. Leaves were syringe inoculated with OD_{600}=0.2 and photographed at 3 dpi.

Fig. S5: Transgenic *A. thaliana* GFP-XopL plants display defects in autophagic degradation
(A) Immunoblot analysis of NBR1 protein levels in transgenic UBQ::GFP-XopL plants or Col-0. Plants were treated with concanamycin A (ConA) for 6 hours. Expression of GFP-XopL was verified with an anti-GFP antibody. Ponceau S staining serves as a loading control.
(B) 5 weeks old *A. thaliana* plants expressing UBQ::GFP-XopL develop an early senescence phenotype reminiscent of autophagy deficient mutants.
(C) Localization analysis of GFP-XopL of transgenic *A. thaliana* UBQ::GFP-XopL #23 line. Image represents single confocal planes from abaxial epidermal cells (bars = 5 μm).
(D) RT-qPCR analysis of *ATG8a* and *NBR1* transcript levels in *Arabidopsis thaliana* GFP or GFP-XopL plants. Values represent mean + SD (n=3) relative to GFP control and were normalized to *PP2A*. Statistical significance (**P*<0.05) was revealed by Student's *t*-test.

Fig. S6: XopL is degraded in the vacuole.
Localization of GFP-XopL in the presence or absence of ConA in transgenic GFP-XopL. DMSO or 0.5 μM ConA was used to treat seedlings, followed by confocal imaging of the roots. GFP-labeled puncta detectable upon ConA treatment indicate XopL accumulation in the vacuole (bars = 20 μm).

Fig. S7: Virus-induced gene silencing of *Joka2* in *N. benthamiana* plants. qRT-PCR analysis of Joka2 mRNA levels in *Joka2* silenced pepper plants. *Actin* expression was used to normalize the expression value in each sample, and relative expression values were determined against pTRV2 control plants (set to 1)**.**

Fig. S8: XopL is ubiquitinated *in planta*.
XopL ubiquitination site at lysine 191 was identified in vivo by LC-MS/MS. GFP-XopL was transiently expressed in *N. benthamiana* and total proteins were subjected to anti-GFP IP followed by trypsin digestion. Ubiquitinated peptides were detected by LC-MS/MS. The spectrum shows the fragmentation pattern of the GlyGly modified peptide ALglKATADLLEDATQPGR corresponding to amino acids 189-205.

Fig. S9: XopL undergoes self-ubiquitination
(A) *In vitro* ubiquitination assay reveals autoubiquitination of XopL. Ubiquitination of MBP-XopL was tested using the Arabidopsis His-AtUBA1 and His-AtUBC8. Lanes 2 to 4 are negative controls. Proteins were separated by SDS-PAGE and detected by immunoblotting using the indicated antibodies. Arrows in the MBP blot indicate higher molecular weight bands of MBP-XopL and autoubiquitination events. The experiment was repeated twice with similar results. **(B)** XopL ubiquitination site at lysine 191 was identified in vitro by LC-MS/MS. GST-XopL was used in an in vitro ubiquitination assay and samples were subjected to trypsin digestion. Ubiquitinated peptides were detected by LC-MS/MS. The spectrum shows the fragmentation pattern of the GlyGly modified peptide ALglKATADLLEDATQPGR corresponding to amino acids 189-205.

Fig. S10: Localization of GFP-XopL$_{K191A}$ in *N. benthamiana*.
Localization analysis of GFP-XopL$_{K191A}$ in *N. benthamiana* leaves. Imaging was performed 2 d after transient expression and images represent single confocal planes from abaxial epidermal cells (bars = 20 µm).

Fig. S11: GFP-XopL$_{K191A}$ is still ubiquitinated in planta.
XopL is ubiquitinated *in planta*. GFP-XopL and GFP-XopL$_{K191A}$ were transiently expressed in *N. benthamiana*. RFP-AIMp was co-infiltrated. Samples were taken 48 hpi, and total proteins (Input) were subjected to immunoprecipitation (IP) with the ubiquitin pan selector, followed by immunoblot analysis of the precipitates using either anti-GFP or anti-ubiquitin antibodies. GFP served as a control. RFP-AIMp expression was verified by an anti-RFP antibody. Asterisk indicates the GFP-XopL full-length protein. The experiment was repeated twice with similar results.

Fig. S12: SH3P2 is conserved in different plant species.
(A) Protein sequence alignment of SH3P2 from different species. The alignment was generated using CLUSTALW2 with default parameters and BoxShade 3.21. Positions of identical and similar sequences are boxed in black and grey, respectively. The following sequences were used to build the alignment: *Arabidopsis thaliana*, *Nicotiana tabacum, Nicotiana benthamiana*, *Solanum lycopersicum*. Phylogentic analysis of the SH3P2 from different plant species.
(B) XopL interacts with SH3P2 from *Nicotiana tabacum* and *Nicotiana benthamiana*. Interaction of XopL with SH3P2 in yeast two-hybrid assays. XopL fused to the GAL4 DNA-binding domain was expressed in combination with SH3P2 fused to the GAL4 activation domain (AD) in yeast strain Y190. Cells were grown on selective media before a LacZ filter assay was performed. The empty AD or BD vector served as negative control. NtSH3P2 = *Nicotiana tabacum* SH3P2, NbSH3P2 = *Nicotiana benthamiana* –LT = yeast growth on medium without Leu and Trp, –HLT = yeast growth on medium lacking His, Leu, and Trp, indicating expression of the HIS3 reporter gene. LacZ, activity of the lacZ reporter gene.

Supp Video 1: XopL/SH3P2 puncta are mobile
Nicotiana benthamiana leaf epidermal cells transiently expressing Venus^{N173}-XopL in combination with AtSH3P2-Venus^{C155}.

Fig. S13: RFP-XopL ΔE3 co-localizes with SH3P2-GFP.
Colocalization analysis of RFP-XopL ΔE3 with SH3P2-GFP in *N. benthamiana* leaves. Imaging was performed 2 d after transient expression and images represent single confocal planes from abaxial epidermal cells (bars = 20 µm).

Fig. S14: Protein levels of GFP-XopL ΔE3 are stabilized by AIMp and ConA treatment.
(A) and (B) Immunoblot analysis of GFP protein levels using anti-GFP antibody. AIMPp was verified by anti-RFP antibody. Plants were treated with concanamycin A (ConA) in (B) for 6 hours. Ponceau staining (PS) serves as a loading control.

Fig. S15: Virus-induced gene silencing of SH3P2 in *N. benthamiana* plants. (A) qRT-PCR analysis of SH3P2 mRNA levels in silenced plants. *Actin* expression was used to normalize the expression value in each sample, and relative expression values were determined against pTRV2 control plants (set to 1)**. (B)** Phenotype of SH3P2-VIGS plants in comparison to the pTRV2 control. Picture was taken 14 dpi.

Fig. S16: Model illustrating the function of XopL

(A) Xenophagy of XopL: Upon delivery of XopL in the plant XopL undergoes self-ubiquitination and possible ubiquitination by an unknown host E3 ligase. Joka2/NBR1 associates with XopL and triggers its degradation via the selective autophagy pathway in the vacuole. **(B) XopL blocks autophagy and self-degradation**: XopL interacts with autophagy component SH3P2 inside the cell and ubiquitinates it to degrade it via the 26S proteasome. Degradation of SH3P2 results in defects of autophagosome delivery into the vacuole and hence suppresses autophagy.

References

1. C. Pohl, I. Dikic, Cellular quality control by the ubiquitin-proteasome system and autophagy. *Science* **366**, 818-822 (2019).
2. R. S. Marshall, R. D. Vierstra, Autophagy: The Master of Bulk and Selective Recycling. *Annual review of plant biology* **69**, 173-208 (2018).
3. H. Hu, S. C. Sun, Ubiquitin signaling in immune responses. *Cell research* **26**, 457-483 (2016).
4. E. H. G. Adams, S. H. Spoel, The ubiquitin-proteasome system as a transcriptional regulator of plant immunity. *Journal of experimental botany* **69**, 4529-4537 (2018).
5. N. Germic, Z. Frangez, S. Yousefi, H. U. Simon, Regulation of the innate immune system by autophagy: neutrophils, eosinophils, mast cells, NK cells. *Cell death and differentiation* **26**, 703-714 (2019).
6. B. Levine, N. Mizushima, H. W. Virgin, Autophagy in immunity and inflammation. *Nature* **469**, 323-335 (2011).
7. Y. Yang, D. J. Klionsky, Autophagy and disease: unanswered questions. *Cell death and differentiation* **27**, 858-871 (2020).
8. S. Üstün, A. Hafrén, D. Hofius, Autophagy as a mediator of life and death in plants. *Current opinion in plant biology* **40**, 122-130 (2017).
9. A. Y. Leary, Z. Savage, Y. Tumtas, T. O. Bozkurt, Contrasting and emerging roles of autophagy in plant immunity. *Current opinion in plant biology* **52**, 46-53 (2019).
10. N. Germic, Z. Frangez, S. Yousefi, H. U. Simon, Regulation of the innate immune system by autophagy: monocytes, macrophages, dendritic cells and antigen presentation. *Cell death and differentiation* **26**, 715-727 (2019).
11. S. Mostowy, Autophagy and bacterial clearance: a not so clear picture. *Cellular microbiology* **15**, 395-402 (2013).
12. J. Huang, J. H. Brumell, Bacteria-autophagy interplay: a battle for survival. *Nature reviews. Microbiology* **12**, 101-114 (2014).
13. L. C. Gomes, I. Dikic, Autophagy in antimicrobial immunity. *Molecular cell* **54**, 224-233 (2014).
14. S. J. van Wijk *et al.*, Fluorescence-based sensors to monitor localization and functions of linear and K63-linked ubiquitin chains in cells. *Molecular cell* **47**, 797-809 (2012).
15. N. Dupont *et al.*, Shigella phagocytic vacuolar membrane remnants participate in the cellular response to pathogen invasion and are regulated by autophagy. *Cell host & microbe* **6**, 137-149 (2009).
16. Y. F. Dagdas *et al.*, An effector of the Irish potato famine pathogen antagonizes a host autophagy cargo receptor. *Elife* **5** (2016).
17. Y. F. Dagdas *et al.*, Host autophagy machinery is diverted to the pathogen interface to mediate focal defense responses against the Irish potato famine pathogen. *Elife* **7** (2018).
18. S. Üstün *et al.*, Bacteria Exploit Autophagy for Proteasome Degradation and Enhanced Virulence in Plants. *The Plant cell* **30**, 668-685 (2018).
19. A. Hafrén *et al.*, Selective autophagy limits cauliflower mosaic virus infection by NBR1-mediated targeting of viral capsid protein and particles. *Proceedings of the*

1369 *National Academy of Sciences of the United States of America* **114**, E2026-E2035
1370 (2017).
1371 20. A. Hafrén *et al.*, Turnip Mosaic Virus Counteracts Selective Autophagy of the Viral
1372 Silencing Suppressor HCpro. *Plant physiology* **176**, 649-662 (2018).
1373 21. M. Khan, D. Seto, R. Subramaniam, D. Desveaux, Oh, the places they'll go! A survey
1374 of phytopathogen effectors and their host targets. *The Plant journal : for cell and*
1375 *molecular biology* **93**, 651-663 (2018).
1376 22. G. Langin, P. Gouguet, S. Üstün, Microbial Effector Proteins - A Journey through the
1377 Proteolytic Landscape. *Trends in microbiology* **28**, 523-535 (2020).
1378 23. M. J. Banfield, Perturbation of host ubiquitin systems by plant pathogen/pest effector
1379 proteins. *Cellular microbiology* **17**, 18-25 (2015).
1380 24. S. Üstün *et al.*, The Proteasome Acts as a Hub for Plant Immunity and Is Targeted by
1381 Pseudomonas Type III Effectors. *Plant physiology* **172**, 1941-1958 (2016).
1382 25. S. Üstün, D. Hofius, Anti- and pro-microbial roles of autophagy in plant-bacteria
1383 interactions. *Autophagy* **14**, 1465-1466 (2018).
1384 26. N. K. Lal *et al.*, Phytopathogen Effectors Use Multiple Mechanisms to Manipulate Plant
1385 Autophagy. *Cell host & microbe* **28**, 558-571 e556 (2020).
1386 27. S. Timilsina *et al.*, Xanthomonas diversity, virulence and plant-pathogen interactions.
1387 *Nature reviews. Microbiology* **18**, 415-427 (2020).
1388 28. S. Üstün, F. Börnke, Interactions of Xanthomonas type-III effector proteins with the
1389 plant ubiquitin and ubiquitin-like pathways. *Frontiers in plant science* **5**, 736 (2014).
1390 29. D. Buttner, Behind the lines-actions of bacterial type III effector proteins in plant cells.
1391 *FEMS microbiology reviews* **40**, 894-937 (2016).
1392 30. Y. Yan, P. Wang, C. He, H. Shi, MeWRKY20 and its interacting and activating
1393 autophagy-related protein 8 (MeATG8) regulate plant disease resistance in cassava.
1394 *Biochemical and biophysical research communications* **494**, 20-26 (2017).
1395 31. H. Zeng *et al.*, Molecular identification of GAPDHs in cassava highlights the
1396 antagonism of MeGAPCs and MeATG8s in plant disease resistance against cassava
1397 bacterial blight. *Plant molecular biology* **97**, 201-214 (2018).
1398 32. N. Adlung *et al.*, Non-host Resistance Induced by the Xanthomonas Effector XopQ Is
1399 Widespread within the Genus Nicotiana and Functionally Depends on EDS1. *Frontiers*
1400 *in plant science* **7**, 1796 (2016).
1401 33. A. N. Dauphinee *et al.*, Chemical Screening Pipeline for Identification of Specific Plant
1402 Autophagy Modulators. *Plant physiology* **181**, 855-866 (2019).
1403 34. P. Pandey *et al.*, The Irish potato famine pathogen subverts host vesicle trafficking to
1404 channel starvation-induced autophagy to the pathogen interface. *bioRxiv*
1405 10.1101/2020.03.20.000117, 2020.2003.2020.000117 (2020).
1406 35. S. Svenning, T. Lamark, K. Krause, T. Johansen, Plant NBR1 is a selective autophagy
1407 substrate and a functional hybrid of the mammalian autophagic adapters NBR1 and
1408 p62/SQSTM1. *Autophagy* **7**, 993-1010 (2011).
1409 36. E. A. Minina et al., Transcriptional stimulation of rate-limiting components of the
1410 autophagic pathway improves plant fitness. *Journal of experimental botany* **69**, 1415-
1411 1432 (2018).
1412 37. J. Gantner, J. Ordon, C. Kretschmer, R. Guerois, J. Stuttmann, An EDS1-SAG101
1413 Complex Is Essential for TNL-Mediated Immunity in Nicotiana benthamiana. *The Plant*
1414 *cell* **31**, 2456-2474 (2019).
1415 38. S. Üstün, V. Bartetzko, F. Börnke, The *Xanthomonas campestris* type III effector XopJ
1416 targets the host cell proteasome to suppress salicylic-acid mediated plant defence. *PLoS*
1417 *pathogens* **9**, e1003427 (2013).

1418 39. C. Lorenz, D. Buttner, Functional characterization of the type III secretion ATPase
1419 HrcN from the plant pathogen *Xanthomonas campestris* pv. *vesicatoria*. *Journal of*
1420 *bacteriology* **191**, 1414-1428 (2009).
1421 40. J. G. Kim, W. Stork, M. B. Mudgett, Xanthomonas type III effector XopD desumoylates
1422 tomato transcription factor SlERF4 to suppress ethylene responses and promote
1423 pathogen growth. *Cell host & microbe* **13**, 143-154 (2013).
1424 41. A. U. Singer *et al.*, A pathogen type III effector with a novel E3 ubiquitin ligase
1425 architecture. *PLoS pathogens* **9**, e1003121 (2013).
1426 42. S. Üstün, F. Börnke, The Xanthomonas campestris type III effector XopJ proteolytically
1427 degrades proteasome subunit RPT6. *Plant physiology* **168**, 107-119 (2015).
1428 43. S. Üstün, V. Bartetzko, F. Börnke, The Xanthomonas effector XopJ triggers a
1429 conditional hypersensitive response upon treatment of N. benthamiana leaves with
1430 salicylic acid. *Frontiers in plant science* **6**, 599 (2015).
1431 44. A. Hafrén, D. Hofius, NBR1-mediated antiviral xenophagy in plant immunity.
1432 *Autophagy* **13**, 2000-2001 (2017).
1433 45. Q. Chai *et al.*, A Mycobacterium tuberculosis surface protein recruits ubiquitin to trigger
1434 host xenophagy. *Nature communications* **10**, 1973 (2019).
1435 46. Y. T. Zheng *et al.*, The adaptor protein p62/SQSTM1 targets invading bacteria to the
1436 autophagy pathway. *J Immunol* **183**, 5909-5916 (2009).
1437 47. J. Zhou *et al.*, NBR1-mediated selective autophagy targets insoluble ubiquitinated
1438 protein aggregates in plant stress responses. *PLoS Genet* **9**, e1003196 (2013).
1439 48. G. Furlan *et al.*, Changes in PUB22 Ubiquitination Modes Triggered by MITOGEN-
1440 ACTIVATED PROTEIN KINASE3 Dampen the Immune Response. *The Plant cell* **29**,
1441 726-745 (2017).
1442 49. P. Albers, S. Üstün, K. Witzel, M. Kraner, F. Börnke, A Remorin from Nicotiana
1443 benthamiana Interacts with the Pseudomonas Type-III Effector Protein HopZ1a and is
1444 Phosphorylated by the Immune-Related Kinase PBS1. *Molecular plant-microbe*
1445 *interactions : MPMI* **32**, 1229-1242 (2019).
1446 50. S. Üstün, P. Konig, D. S. Guttman, F. Börnke, HopZ4 from Pseudomonas syringae, a
1447 Member of the HopZ Type III Effector Family from the YopJ Superfamily, Inhibits the
1448 Proteasome in Plants. *Molecular plant-microbe interactions : MPMI* **27**, 611-623
1449 (2014).
1450 51. X. Zhuang *et al.*, A BAR-domain protein SH3P2, which binds to phosphatidylinositol
1451 3-phosphate and ATG8, regulates autophagosome formation in Arabidopsis. *The Plant*
1452 *cell* **25**, 4596-4615 (2013).
1453 52. X. Zhuang, L. Jiang, Autophagosome biogenesis in plants: roles of SH3P2. *Autophagy*
1454 **10**, 704-705 (2014).
1455 53. M. K. Nagel *et al.*, Arabidopsis SH3P2 is an ubiquitin-binding protein that functions
1456 together with ESCRT-I and the deubiquitylating enzyme AMSH3. *Proceedings of the*
1457 *National Academy of Sciences of the United States of America* **114**, E7197-E7204
1458 (2017).
1459 54. J. L. Erickson, N. Adlung, C. Lampe, U. Bonas, M. H. Schattat, The Xanthomonas
1460 effector XopL uncovers the role of microtubules in stromule extension and dynamics in
1461 Nicotiana benthamiana. *The Plant journal : for cell and molecular biology* **93**, 856-870
1462 (2018).
1463 55. Y. Jiao, J. Sun, Bacterial Manipulation of Autophagic Responses in Infection and
1464 Inflammation. *Front Immunol* **10**, 2821 (2019).
1465 56. N. K. Kushwaha, A. Hafrén, D. Hofius, Autophagy-virus interplay in plants: from
1466 antiviral recognition to proviral manipulation. *Molecular plant pathology* **20**, 1211-
1467 1216 (2019).

1468 57. B. Orosa *et al.*, Plant proteostasis - shaping the proteome: a research community aiming
1469 to understand molecular mechanisms that control protein abundance. *The New*
1470 *phytologist* **227**, 1028-1033 (2020).
1471 58. A. Y. Leary *et al.*, Modulation of plant autophagy during pathogen attack. *Journal of*
1472 *experimental botany* **69**, 1325-1333 (2018).
1473 59. J. G. Kim *et al.*, XopD SUMO protease affects host transcription, promotes pathogen
1474 growth, and delays symptom development in Xanthomonas-infected tomato leaves. *The*
1475 *Plant cell* **20**, 1915-1929 (2008).
1476 60. G. Ahn *et al.*, SH3 Domain-Containing Protein 2 Plays a Crucial Role at the Step of
1477 Membrane Tubulation during Cell Plate Formation. *The Plant cell* **29**, 1388-1405
1478 (2017).
1479 61. Y. Gu, R. Zavaliev, X. Dong, Membrane Trafficking in Plant Immunity. *Molecular*
1480 *plant* **10**, 1026-1034 (2017).
1481 62. H. D. Lenz *et al.*, Autophagy differentially controls plant basal immunity to biotrophic
1482 and necrotrophic pathogens. *The Plant journal : for cell and molecular biology* **66**, 818-
1483 830 (2011).
1484 63. H. B. Yu *et al.*, Autophagy facilitates Salmonella replication in HeLa cells. *mBio* **5**,
1485 e00865-00814 (2014).
1486 64. J. Huang *et al.*, Antibacterial autophagy occurs at PI(3)P-enriched domains of the
1487 endoplasmic reticulum and requires Rab1 GTPase. *Autophagy* **7**, 17-26 (2011).
1488 65. F. Li *et al.*, Beclin1 restricts RNA virus infection in plants through suppression and
1489 degradation of the viral polymerase. *Nature communications* **9**, 1268 (2018).
1490 66. F. Li *et al.*, A plant RNA virus activates selective autophagy in a UPR-dependent
1491 manner to promote virus infection. *The New phytologist* **228**, 622-639 (2020).
1492 67. V. Kirkin, T. Lamark, T. Johansen, I. Dikic, NBR1 cooperates with p62 in selective
1493 autophagy of ubiquitinated targets. *Autophagy* **5**, 732-733 (2009).
1494 68. F. S. Mesquita *et al.*, The Salmonella deubiquitinase SseL inhibits selective autophagy
1495 of cytosolic aggregates. *PLoS pathogens* **8**, e1002743 (2012).
1496 69. L. Lou, P. Zhang, R. Piao, Y. Wang, Salmonella Pathogenicity Island 1 (SPI-1) and Its
1497 Complex Regulatory Network. *Frontiers in cellular and infection microbiology* **9**, 270
1498 (2019).
1499 70. T. Maculins, E. Fiskin, S. Bhogaraju, I. Dikic, Bacteria-host relationship: ubiquitin
1500 ligases as weapons of invasion. *Cell research* **26**, 499-510 (2016).
1501 71. Y. Zhang, W. Higashide, S. Dai, D. M. Sherman, D. Zhou, Recognition and
1502 ubiquitination of Salmonella type III effector SopA by a ubiquitin E3 ligase, HsRMA1.
1503 *The Journal of biological chemistry* **280**, 38682-38688 (2005).
1504 72. T. Kubori, J. E. Galan, Temporal regulation of salmonella virulence effector function
1505 by proteasome-dependent protein degradation. *Cell* **115**, 333-342 (2003).
1506 73. G. Furlan, J. Klinkenberg, M. Trujillo, Regulation of plant immune receptors by
1507 ubiquitination. *Frontiers in plant science* **3**, 238 (2012).
1508 74. J. R. Rohde, A. Breitkreutz, A. Chenal, P. J. Sansonetti, C. Parsot, Type III secretion
1509 effectors of the IpaH family are E3 ubiquitin ligases. *Cell host & microbe* **1**, 77-83
1510 (2007).
1511 75. J. Noad *et al.*, LUBAC-synthesized linear ubiquitin chains restrict cytosol-invading
1512 bacteria by activating autophagy and NF-kappaB. *Nat Microbiol* **2**, 17063 (2017).
1513 76. Kovach, M., et. al., Four new derivatives of the broad-host-range cloning vector
1514 pBBR1MCS, carrying different antibiotic-resistance cassettes. *Gene* **166**, 175-6 (1995)
1515 77. C. Grefen et al., A ubiquitin-10 promoter-based vector set for fluorescent protein
1516 tagging facilitates temporal stability and native protein distribution in transient and
1517 stable expression studies. *The Plant journal*: for cell and molecular biology **64**, 355-365
1518 (2010).

1519 78. T. Nakagawa et al., Development of series of gateway binary vectors, pGWBs, for
1520 realizing efficient construction of fusion genes for plant transformation. J Biosci Bioeng
1521 104, 34-41 (2007).
1522 79. S. J. Clough, A. F. Bent, Floral dip: a simplified method for Agrobacterium-mediated
1523 transformation of Arabidopsis thaliana. *The Plant journal*: for cell and molecular
1524 biology **16**, 735-743 (1998).
1525 80. N. Borchert et al., Proteogenomics of *Pristionchus pacificus* reveals distinct proteome
1526 structure of nematode models. *Genome Res* **20**, 837-846 (2010).
1527 81. K. Kliza et al., Internally tagged ubiquitin: a tool to identify linear polyubiquitin-
1528 modified proteins by mass spectrometry. *Nature methods* **14**, 504-512 (2017).
1529 82. B. Schwanhausser et al., Global quantification of mammalian gene expression control.
1530 *Nature* **473**, 337-342 (2011).
1531

1532 **Supporting information**

1533

1534 **Figure S1:** Virus-induced gene silencing of *ATG7* in *N. benthamiana* plants.
1535 **Figure S2:** Suppression of autophagy is enhanced by T3Es**.**
1536 **Figure S3:** Screening for Xanthomonas T3Es with altered autophagic flux.
1537 **Figure S4:** XopL is an essential virulence factor
1538 **Figure S5:** Transgenic *A. thaliana* GFP-XopL plants display defects in autophagic degradation.
1539 **Figure S6:** XopL is degraded in the vacuole.
1540 **Figure S7**: Confirmation of efficient silencing of NBR1/Joka2.
1541 **Figure S8:** XopL is ubiquitinated *in planta*.
1542 **Figure S9:** XopL undergoes self-ubiquitination.
1543 **Figure S10:** Localization of GFP-XopL$_{K191A}$ in *N. benthamiana*.
1544 **Figure S11**: GFP-XopL$_{K191A}$ is still ubiquitinated in planta.
1545 **Figure S12:** SH3P2 is conserved in different plant species.
1546 **Supplemental Video 1:** XopL/SH3P2 puncta are mobile.
1547 **Figure S13:** RFP-XopL ΔE3 co-localizes with SH3P2-GFP.
1548 **Figure S14:** Protein levels of GFP-XopL ΔE3 are stabilized by AIMp and ConA treatment.
1549 **Figure S15:** Virus-induced gene silencing of SH3P2 in *N. benthamiana* plants.
1550 **Figure S16:** Model illustrating the function of XopL.
1551 **Supplemental Table 1**: Primers used in manuscript.

1552

1553 **Supplemental Figure 1**

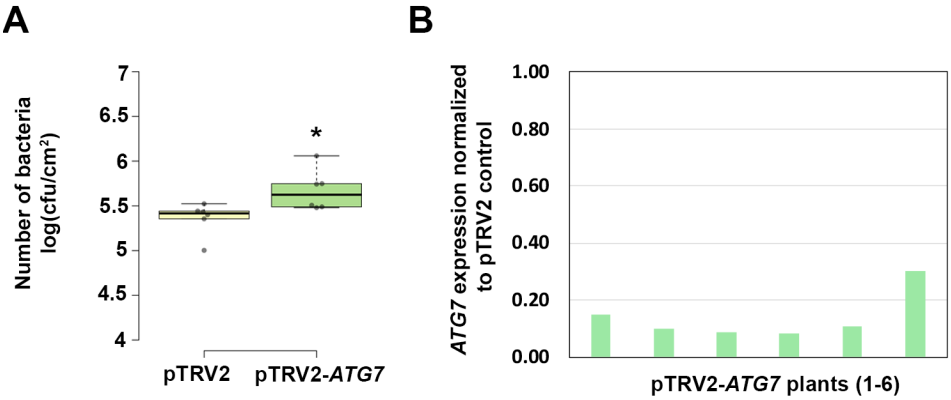

1554
1555 **Fig. S1: Virus-induced gene silencing of *ATG7* in *N. benthamiana* plants.**
1556 **(A)** Growth of Xcv *ΔxopQ* in *N. benthamiana* plants silenced for *ATG7* (pTRV2-*ATG7*)
1557 compared to control plants (pTRV2). Leaves were dip-inoculated with a bacteria suspension at
1558 OD_{600} = 0.2 and bacteria were quantified at 6 dpi. Data represent the mean SD (n = 6).
1559 Significant differences were calculated using Student's *t-test* and are indicated by *, $P < 0.05$.
1560 The experiment was repeated twice with similar trends.
1561 **(B)** qRT-PCR analysis of *ATG7* mRNA levels in silenced pepper plants. *Actin* expression was
1562 used to normalize the expression value in each sample, and relative expression values were
1563 determined against pTRV2 control plants, which was set to 1**.**

1564
1565
1566

1567 **Supplemental Figure 2**

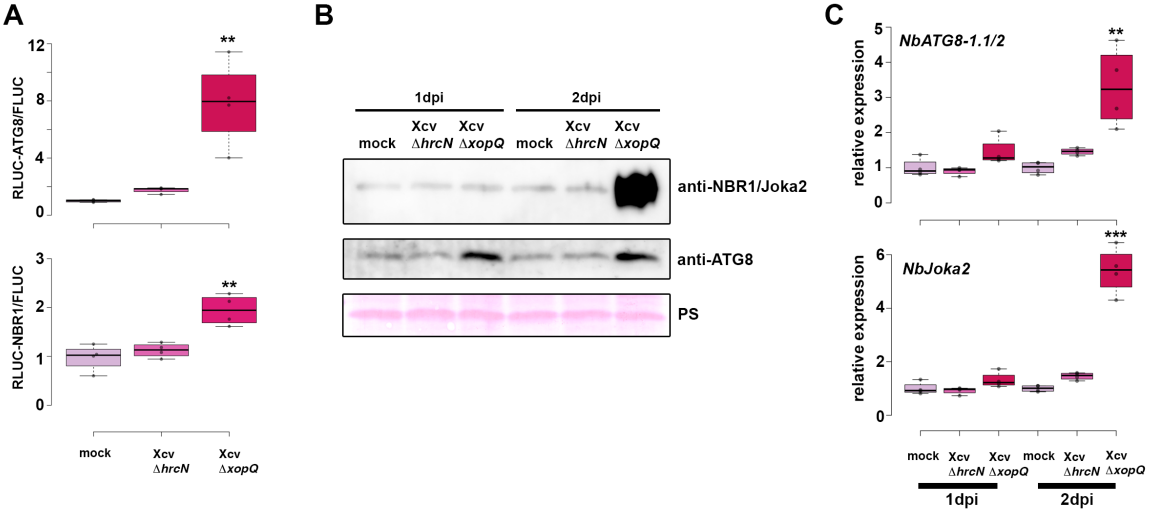

1568
1569 **Fig. S2: Suppression of autophagy is enhanced by T3Es.**

1570 **(A)** Autophagic flux determined by quantitative dual-luciferase assay. RLUC-ATG8a or
1571 RLUC-NBR1 constructs were coexpressed with internal control FLUC in *N. benthamiana*. Xcv
1572 *ΔxopQ* and *ΔhrcN* were co-infiltrated with Agrobacteria containing the respective constructs.
1573 Renilla and Firefly luciferase activities were simultaneously measured in leaf extracts at 48 h
1574 post- infiltration using the dual-luciferase system. Values represent the mean ratio of RLUC-
1575 ATG8a and FLUC activities and error bars show SD (n=4). Statistical significance (**P<0.01)
1576 was revealed by Student's *t*-test. The experiment was repeated 2 times with similar results.
1577 **(B)** Immunoblot analysis of NBR1 and ATG8 protein levels in Xcv *ΔxopQ, ΔhrcN* or mock
1578 infected *N. benthamiana* plants at 1 and 2dpi. Ponceau Staining (PS) served as a loading control.
1579 The experiment was repeated twice with similar results.
1580 **(C)** RT-qPCR analysis of *NbATG8-1.1/2, NbATG8-2.1/2* and *NbJoka2* transcript levels upon
1581 challenge of *N. benthamiana* plants with Xcv *ΔxopQ* and *ΔhrcN* for 1 and 2 dpi compared to
1582 mock infected plants. Values represent mean + SD (n=4) relative to mock control of respective
1583 time point and were normalized to *PP2A*. Statistical significance (**$P < 0.01$, *** $P < 0.001$)
1584 was revealed by Student's *t*-test.
1585
1586 **Supplemental Figure 3**

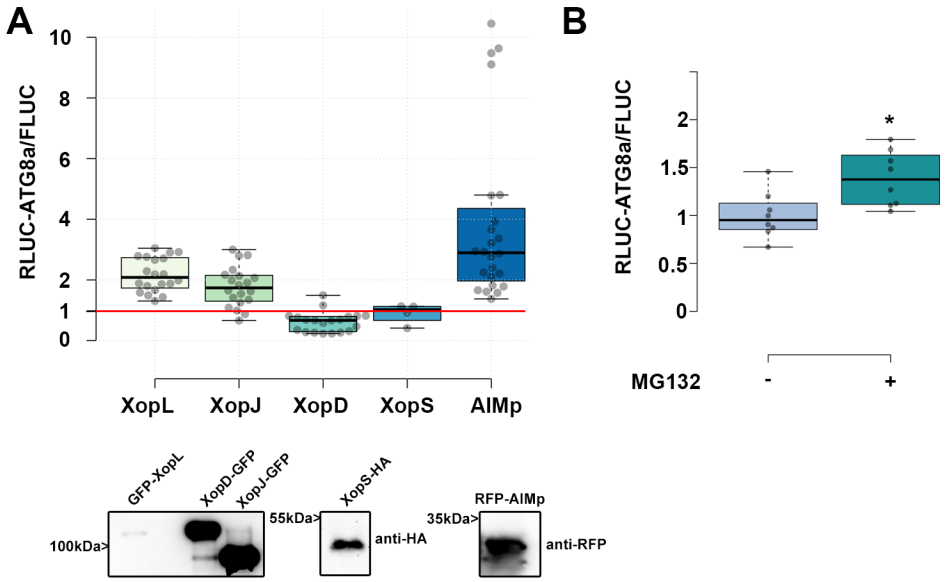

1587
1588

1589 **Fig. S3: Screening for Xanthomonas T3Es with altered autophagic flux.**
1590 **(A)** RLUC-ATG8a constructs were coexpressed with internal control FLUC in *N. benthamiana*.
1591 XopL, XopJ, XopD and XopS were co-infiltrated with the RLUC/FLUC mixture. Renilla and
1592 Firefly luciferase activities were simultaneously measured in leaf extracts at 48 h post-
1593 infiltration using the dual-luciferase system. Values represent the mean ratio of RLUC-ATG8a
1594 and FLUC activities and error bars show SD (XopL, XopJ, XopD, AIMp; n=20; XopS n=4).
1595 GFP served as a control and was set to 1. Expression of T3Es and RFP-AIMp were verified
1596 with the indicated antibodies. **(B)** RLUC-ATG8a constructs were coexpressed with internal
1597 control FLUC in *N. benthamiana*. Plants were treated with MG132 for 6 hours prior
1598 measurement. Values represent the mean ratio of RLUC-ATG8a and FLUC activities and error
1599 bars show SD (n=8). Statistical significance (* $P < 0.5$) was revealed by Student's *t*-test.
1600
1601 **Supplemental Figure 4**

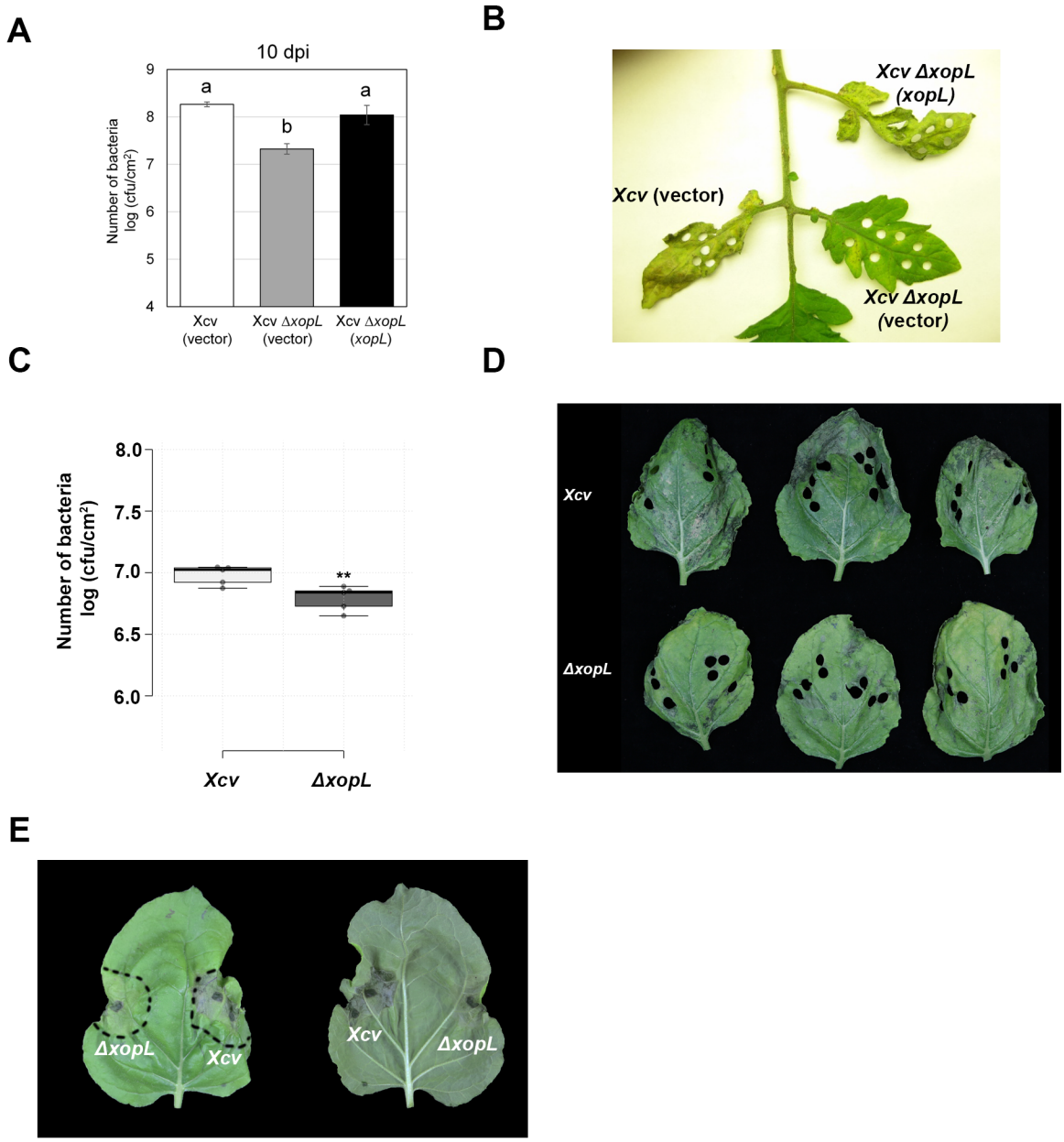

1602
1603 **Fig. S4: XopL is an essential virulence factor**
1604 **(A)** Growth of Xcv 85-10 (vector) (white bar), Xcv 85-10 Δ*xopL* (vector) (grey bar), and Xcv
1605 85-10 Δ*xopL* (*xopL*) (black bar) strains in tomato VF36 leaves. Leaves were dipped in a 2 x 10^8

CFU/mL suspension of bacteria. The number of bacteria in each leaf was quantified at 10 dpi. Data points represent mean $\log_{10}$ colony-forming units per cm^2 ± SD of three plants. Different letters above bars indicate statistically significant (Tukey's honestly significant difference (HSD) test, $P < 0.05$) differences between samples. Vector = pBBR1MCS-2.
(B) Delayed disease symptom development in tomato leaves inoculated with *Xcv* or *Xcv* Δ*xopL*. Tomato leaves inoculated with strains described in (A) were photographed at 14 dpi.
(C) Growth of Xcv 85-10, Xcv 85-10 Δ*xopL* strains in *roq1 N. benthamiana* leaves. Leaves were dipped in a 2 x 10^8 CFU/mL suspension of bacteria. The number of bacteria in each leaf was quantified at 10 dpi. Data represent the mean SD (n = 5). Significant differences were calculated using Student's *t-test* and are indicated by **, $P < 0.01$. The experiment was repeated twice with similar trends.

Supplemental Figure 5

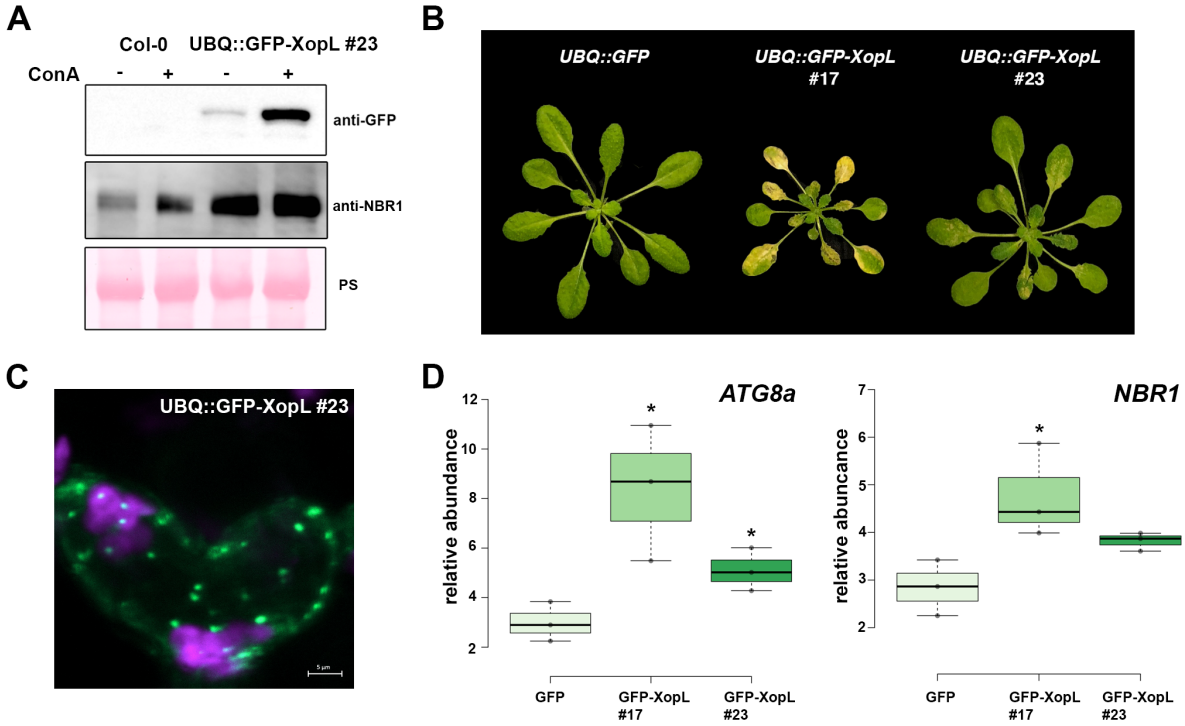

Fig. S5: Transgenic *A. thaliana* GFP-XopL plants display defects in autophagic degradation

(A) Immunoblot analysis of NBR1 protein levels in transgenic UBQ::GFP-XopL plants or Col-0. Plants were treated with concanamycin A (ConA) for 6 hours. Expression of GFP-XopL was verified with an anti-GFP antibody. Ponceau S staining serves as a loading control.
(B) 5 weeks old *A. thaliana* plants expressing UBQ::GFP-XopL develop an early senescence phenotype reminiscent of autophagy deficient mutants.
(C) Localization analysis of GFP-XopL of transgenic *A. thaliana* UBQ::GFP-XopL #23 line. Image represents single confocal planes from abaxial epidermal cells (bars = 5 µm).
(D) RT-qPCR analysis of *ATG8a* and *NBR1* transcript levels in *Arabidopsis thaliana* GFP or GFP-XopL plants. Values represent mean + SD (n=3) relative to GFP control and were normalized to *PP2A*. Statistical significance (*P<0.05) was revealed by Student's *t*-test.

1638 **Supplemental Figure 6**

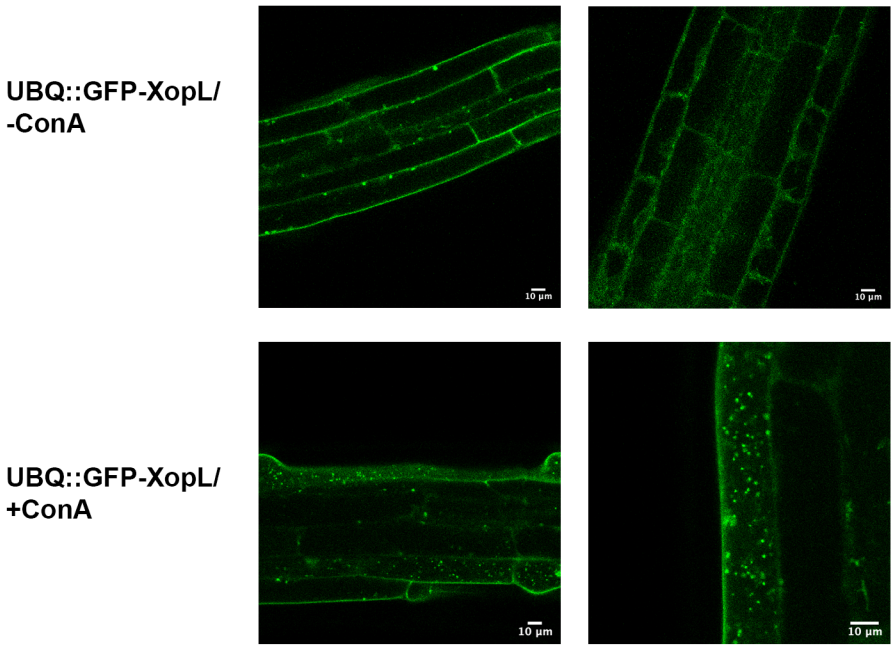

1639
1640 **Fig. S6: XopL is degraded in the vacuole**.
1641 Localization of GFP-XopL in the presence or absence of ConA in transgenic GFP-XopL.
1642 DMSO or 0.5 µM ConA was used to treat seedlings, followed by confocal imaging of the roots.
1643 GFP-labeled puncta detectable upon ConA treatment indicate XopL accumulation in the
1644 vacuole (bars = 20 µm).
1645
1646 **Supplemental Figure 7**

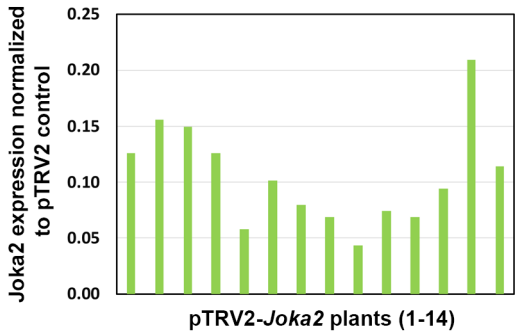

1647
1648 **Fig. S7: Virus-induced gene silencing of *Joka2* in *N. benthamiana* plants.** qRT-PCR analysis
1649 of Joka2 mRNA levels in *Joka2* silenced pepper plants. *Actin* expression was used to normalize
1650 the expression value in each sample, and relative expression values were determined against
1651 pTRV2 control plants (set to 1)**.**
1652
1653 **Supplemental Figure 8**
1654

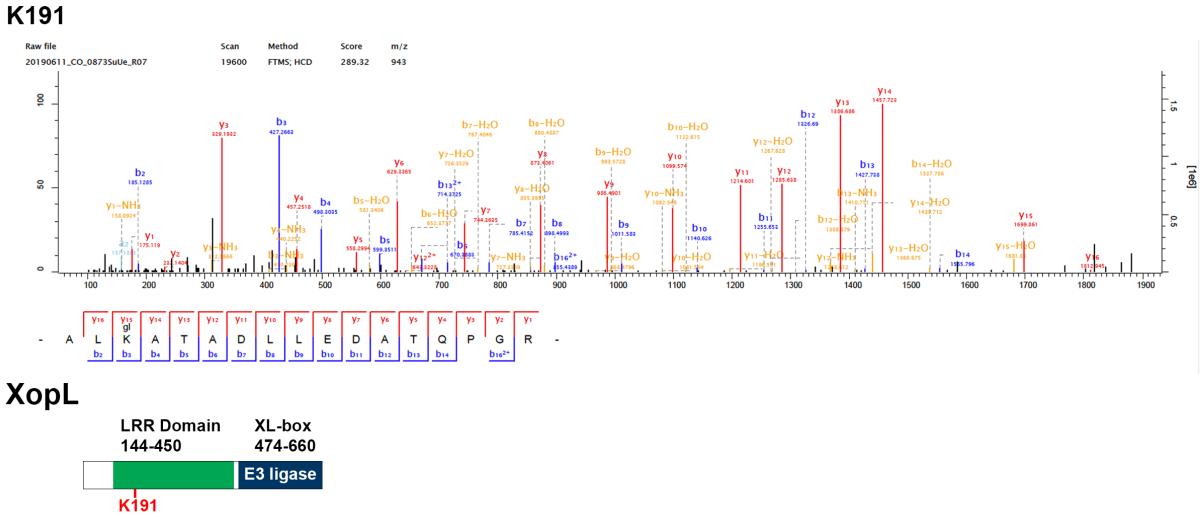

Fig. S8: XopL is ubiquitinated *in planta*.
XopL ubiquitination site at lysine 191 was identified in vivo by LC-MS/MS. GFP-XopL was transiently expressed in *N. benthamiana* and total proteins were subjected to anti-GFP IP followed by trypsin digestion. Ubiquitinated peptides were detected by LC-MS/MS. The spectrum shows the fragmentation pattern of the GlyGly modified peptide ALglKATADLLEDATQPGR corresponding to amino acids 189-205.

Supplemental Figure 9

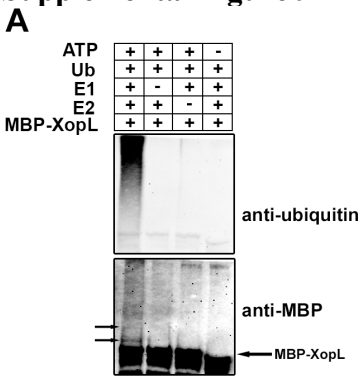

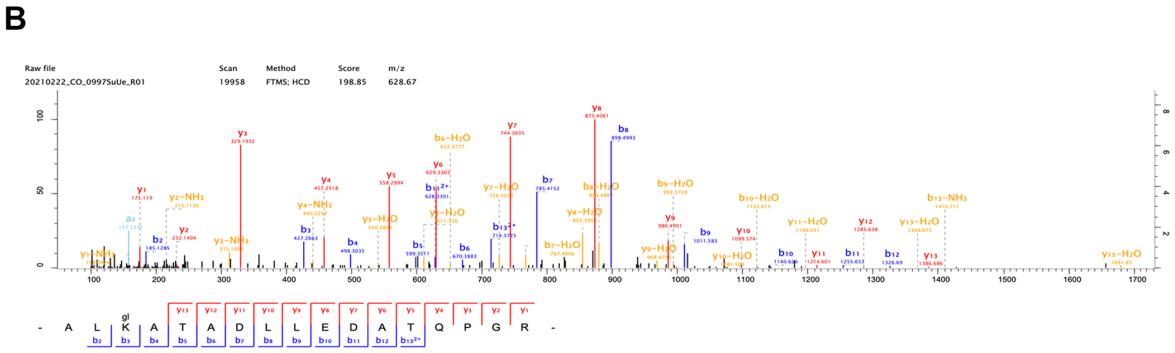

Fig. S9: XopL undergoes self-ubiquitination
(A) *In vitro* ubiquitination assay reveals autoubiquitination of XopL. Ubiquitination of MBP-XopL was tested using the Arabidopsis His-AtUBA1 and His-AtUBC8. Lanes 2 to 4 are negative controls. Proteins were separated by SDS-PAGE and detected by immunoblotting using the indicated antibodies. Arrows in the MBP blot indicate higher molecular weight bands of MBP-XopL and autoubiquitination events. The experiment was repeated twice with similar

results. **(B)** XopL ubiquitination site at lysine 191 was identified in vitro by LC-MS/MS. GST-XopL was used in an in vitro ubiquitination assay and samples were subjected to trypsin digestion. Ubiquitinated peptides were detected by LC-MS/MS. The spectrum shows the fragmentation pattern of the GlyGly modified peptide ALglKATADLLEDATQPGR corresponding to amino acids 189-205.

Supplemental Figure 10

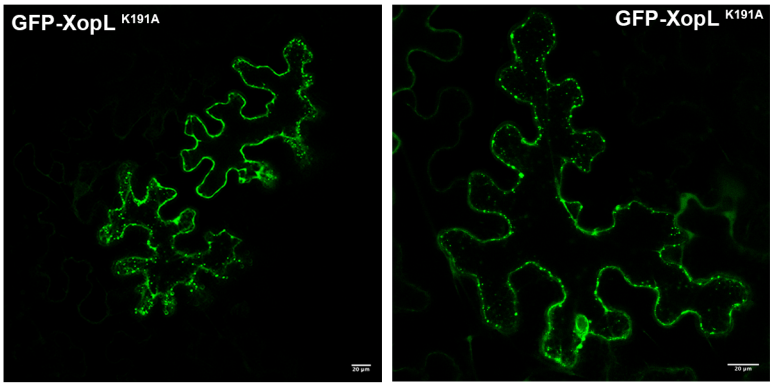

Fig. S10: Localization of GFP-XopL$_{K191A}$ in *N. benthamiana*.
Localization analysis of GFP-XopL$_{K191A}$ in *N. benthamiana* leaves. Imaging was performed 2 d after transient expression and images represent single confocal planes from abaxial epidermal cells (bars = 20 µm).

Supplemental Figure 11

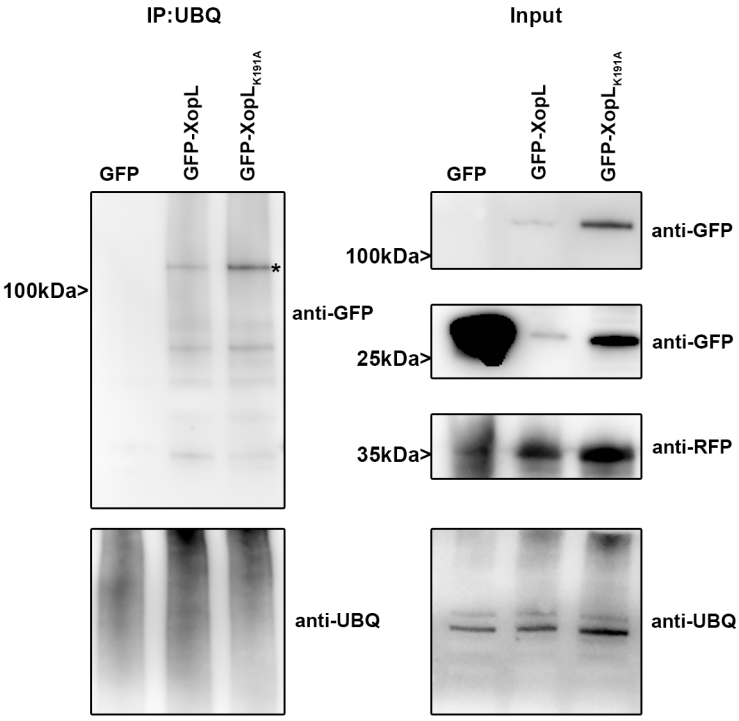

Fig. S11: GFP-XopL$_{K191A}$ is still ubiquitinated in planta.
XopL is ubiquitinated *in planta*. GFP-XopL and GFP-XopL$_{K191A}$ were transiently expressed in *N. benthamiana*. RFP-AIMp was co-infiltrated. Samples were taken 48 hpi, and total proteins (Input) were subjected to immunoprecipitation (IP) with the ubiquitin pan selector, followed by immunoblot analysis of the precipitates using either anti-GFP or anti-ubiquitin antibodies. GFP served as a control. RFP-AIMp expression was verified by an anti-RFP antibody. Asterisk

indicates the GFP-XopL full-length protein. The experiment was repeated twice with similar results.

Supplemental Figure 12

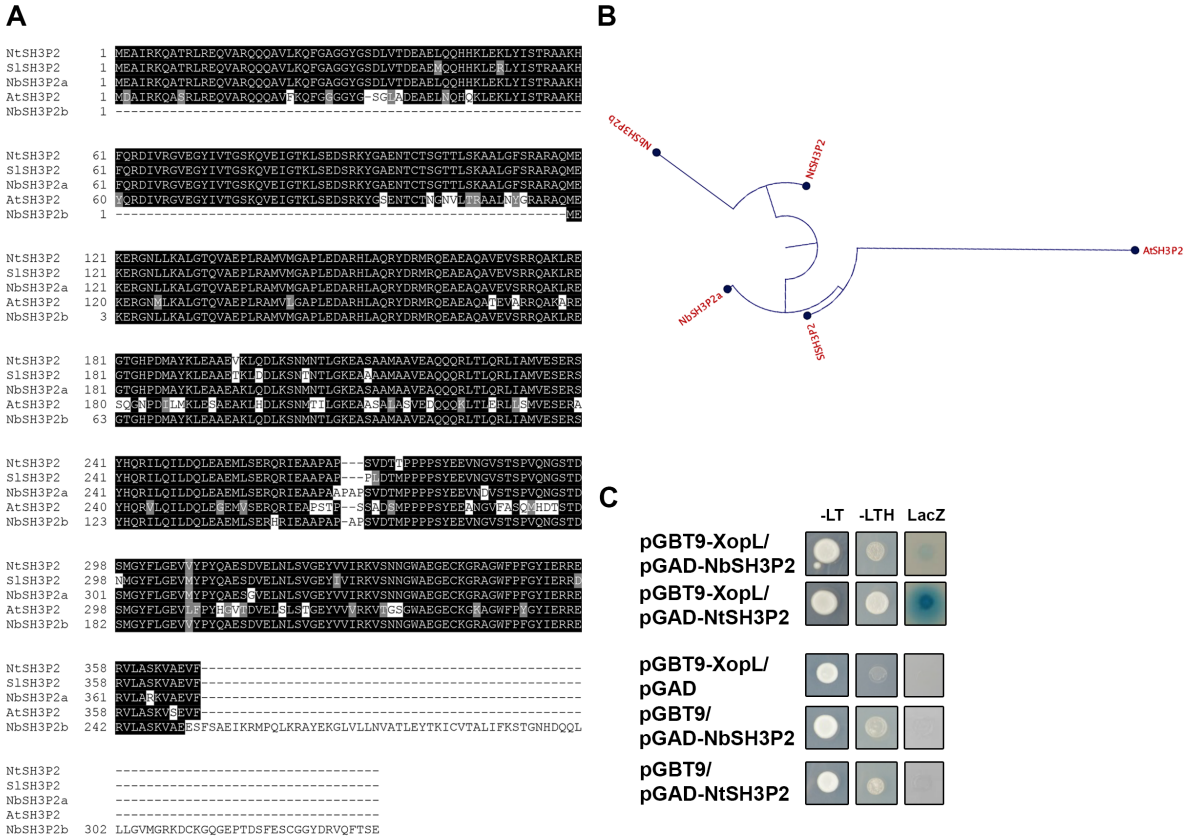

Fig. S12: SH3P2 is conserved in different plant species.
(A) Protein sequence alignment of SH3P2 from different species. The alignment was generated using CLUSTALW2 with default parameters and BoxShade 3.21. Positions of identical and similar sequences are boxed in black and grey, respectively. The following sequences were used to build the alignment: *Arabidopsis thaliana*, *Nicotiana tabacum, Nicotiana benthamiana*, *Solanum lycopersicum*. Phylogentic analysis of the SH3P2 from different plant species.
(B) XopL interacts with SH3P2 from *Nicotiana tabacum* and *Nicotiana benthamiana*. Interaction of XopL with SH3P2 in yeast two-hybrid assays. XopL fused to the GAL4 DNA-binding domain was expressed in combination with SH3P2 fused to the GAL4 activation domain (AD) in yeast strain Y190. Cells were grown on selective media before a LacZ filter assay was performed. The empty AD or BD vector served as negative control. NtSH3P2 = *Nicotiana tabacum* SH3P2, NbSH3P2 = *Nicotiana benthamiana* –LT = yeast growth on medium without Leu and Trp, –HLT = yeast growth on medium lacking His, Leu, and Trp, indicating expression of the HIS3 reporter gene. LacZ, activity of the lacZ reporter gene.

1713 **Supplemental Figure 13**

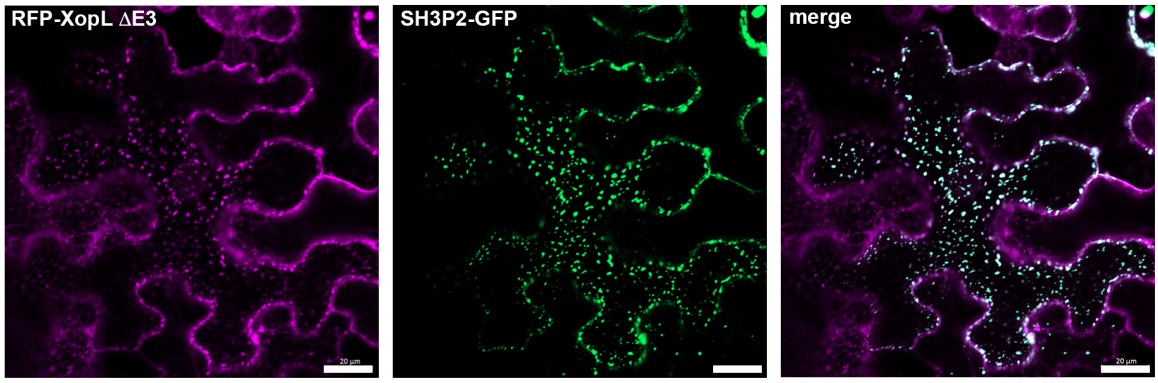

1714
1715 **Fig. S13: RFP-XopL ΔE3 co-localizes with SH3P2-GFP.**
1716 Colocalization analysis of RFP-XopL ΔE3 with SH3P2-GFP in *N. benthamiana* leaves.
1717 Imaging was performed 2 d after transient expression and images represent single confocal
1718 planes from abaxial epidermal cells (bars = 20 µm).
1719
1720 **Supplemental Figure 14**

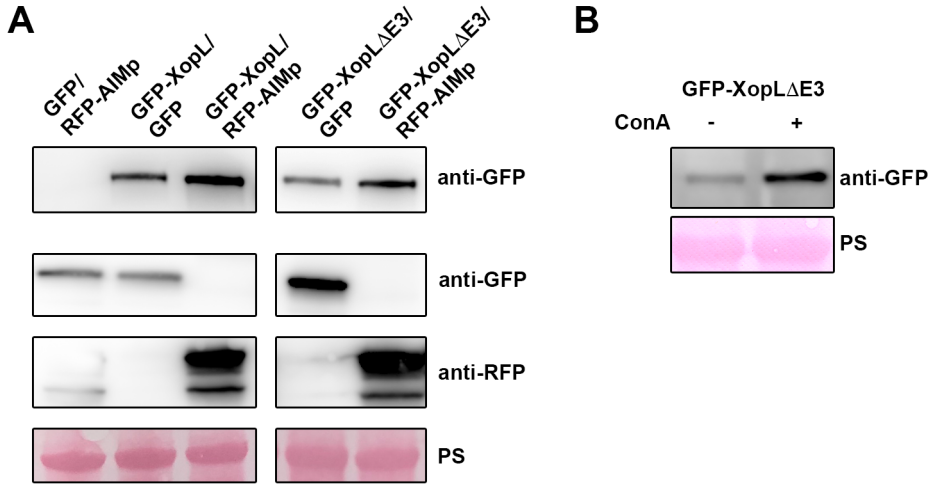

1721
1722 **Fig. S14: Protein levels of GFP-XopL ΔE3 are stabilized by AIMp and ConA treatment.**
1723 **(A) and (B)** Immunoblot analysis of GFP protein levels using anti-GFP antibody. AIMPp was
1724 verified by anti-RFP antibody. Plants were treated with concanamycin A (ConA) in (B) for 6
1725 hours. Ponceau staining (PS) serves as a loading control.
1726
1727 **Supplemental Figure 15**

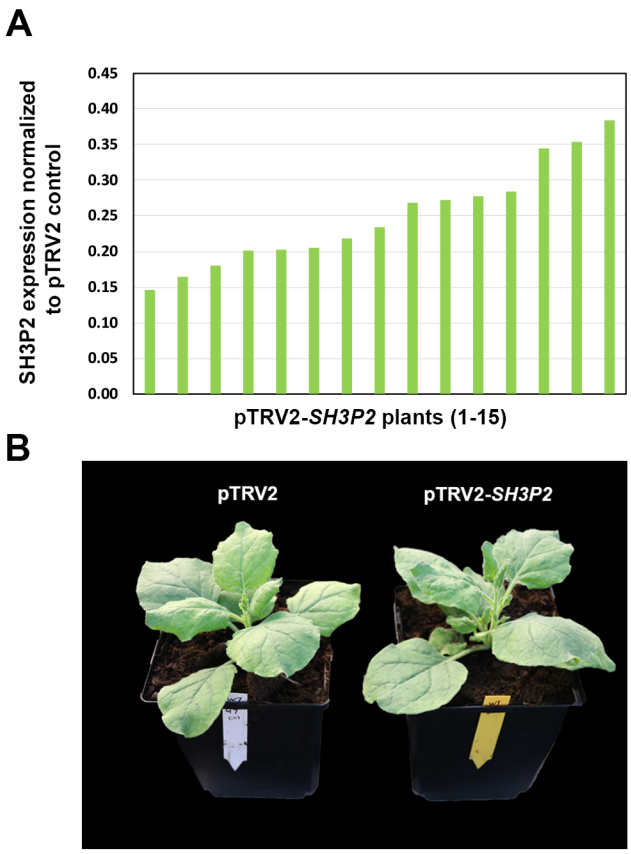

Fig. S15: Virus-induced gene silencing of SH3P2 in *N. benthamiana* plants. (A) qRT-PCR analysis of SH3P2 mRNA levels in silenced plants. *Actin* expression was used to normalize the expression value in each sample, and relative expression values were determined against pTRV2 control plants (set to 1)**. (B)** Phenotype of SH3P2-VIGS plants in comparison to the pTRV2 control. Picture was taken 14 dpi.

1735 **Supplemental Figure 16**

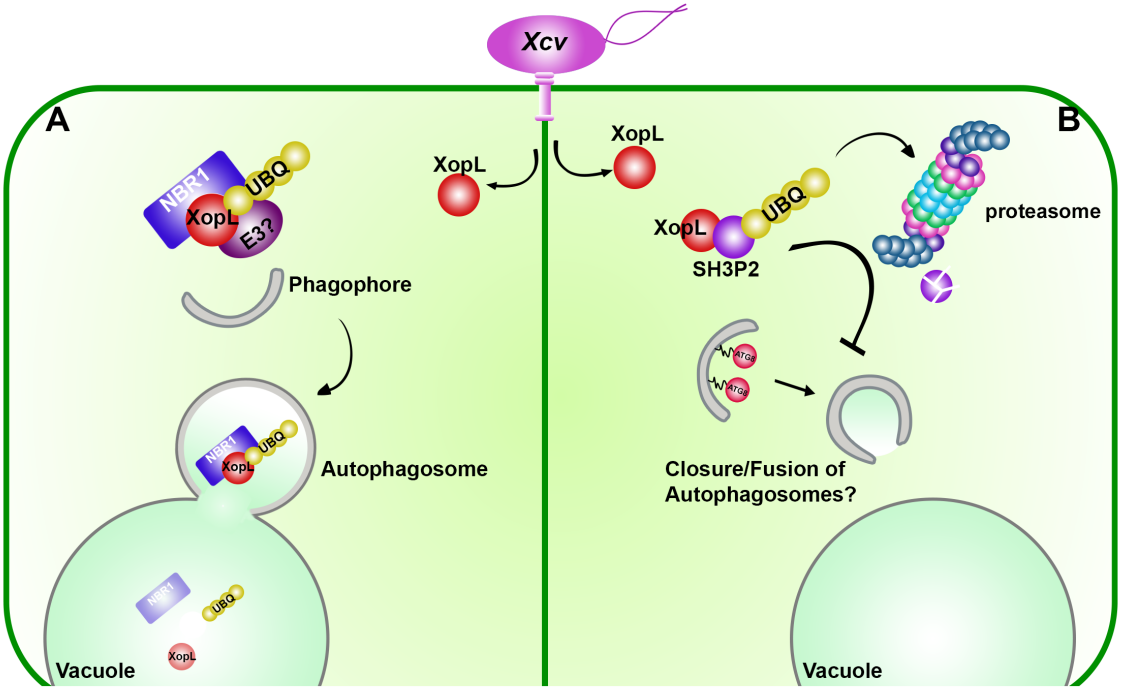

1736
1737 **Fig. S16: Model illustrating the function of XopL**
1738 **(A) Xenophagy of XopL:** Upon delivery of XopL in the plant XopL undergoes self-
1739 ubiquitination and possible ubiquitination by an unknown host E3 ligase. Joka2/NBR1
1740 associates with XopL and triggers its degradation via the selective autophagy pathway in the
1741 vacuole. **(B) XopL blocks autophagy and self-degradation**: XopL interacts with autophagy
1742 component SH3P2 inside the cell and ubiquitinates it to degrade it via the 26S proteasome.
1743 Degradation of SH3P2 results in defects of autophagosome delivery into the vacuole and hence
1744 suppresses autophagy.